energies

MDPI

Article

A Methodology for Assembling Future Weather Files Including Heatwaves for Building Thermal Simulations from the European Coordinated Regional Downscaling Experiment (EURO-CORDEX) Climate Data

Anaïs Machard [1,2,*], Christian Inard [1], Jean-Marie Alessandrini [2], Charles Pelé [2] and Jacques Ribéron [3]

[1] Laboratoire des Sciences de l'Ingénieur pour l'Environnement (LASIE, UMR CNRMS 7356), La Rochelle Université, 23 Avenue Albert Einstein, 17000 La Rochelle, France; christian.inard@univ-lr.fr
[2] Département Energie et Environnement, Centre Scientifique et Technique du Bâtiment (CSTB), 84 Avenue Jean Jaurès, Champs-sur-Marne, 77447 Marne-la-Vallée CEDEX 2, France; jean-marie.ALESSANDRINI@cstb.fr (J.-M.A.); Charles.PELE@cstb.fr (C.P.)
[3] Département Santé et Confort, Centre Scientifique et Technique du Bâtiment (CSTB), 84 Avenue Jean Jaurès, Champs-sur-Marne, 77447 Marne-la-Vallée CEDEX 2, France; jacques.RIBERON@cstb.fr
* Correspondence: anais.machard@univ-lr.fr

Received: 2 April 2020; Accepted: 24 April 2020; Published: 2 July 2020

Abstract: With increasing mean and extreme temperatures due to climate change, it becomes necessary to use—not only future typical conditions—but future heatwaves in building thermal simulations as well. Future typical weather files are widespread, but few researchers have put together methodologies to reproduce future extreme conditions. Furthermore, climate uncertainties need to be considered and it is often difficult due to the lack of data accessibility. In this article, we propose a methodology to re-assemble future weather files—ready-to-use for building simulations—using data from the European Coordinated Regional Downscaling Experiment (EURO-CORDEX) dynamically downscaled regional climate multi-year projections. It is the first time that this database is used to assemble weather files for building simulations because of its recent availability. Two types of future weather files are produced: typical weather years (TWY) and heatwave events (HWE). Combined together, they can be used to fully assess building resilience to overheating in future climate conditions. A case study building in Paris is modelled to compare the impact of the different weather files on the indoor operative temperature of the building. The results confirm that it is better to use multiple types of future weather files, climate models, and or scenarios to fully grasp climate projection uncertainties.

Keywords: climate change; climate data; future weather files; heatwaves; regional climate models; climate uncertainties; EURO-CORDEX; multi-year projections; building simulation; overheating risk; thermal comfort; heat stress

1. Introduction

Using future climate data for building energy simulation has been of interest to the research community for the past twenty years. However, building practitioners, nowadays, continue to use climate data based on historical weather datasets. Considering warming temperatures as a result of climate change in the near future, using only historical datasets for building thermal simulations will soon be outdated. In fact, global mean temperature has already increased by around +1.5 °C–2 °C compared to pre-industrial conditions [1]. The use of historical typical weather years becomes

questionable, as heatwaves have already proven to happen more often. Unfortunately, it is expected that their frequency and duration will only intensify towards the end of this century [2–5]. In recent years, heatwaves had adverse effects on the population, especially in cities exacerbated with the urban heat island (UHI) effect. In Europe, the well-known deadly 2003 heatwave was responsible for 15,000 extra-mortalities [6–8].

Future heatwaves will cause different problems in buildings, depending on local construction practices. In countries where buildings are equipped with air-conditioning, there is a high risk of increased energy related cooling consumption and power shortages during future heatwaves. Furthermore, in countries where air-conditioning has not penetrated yet, it might become common during this century, due to population increase, income growth, increase in comfort requirements, technological improvements, diminution of purchase costs, the UHI effect, the "fear of heatwaves", and climate change [9,10]. A vivid illustration of this is in China, for which air-conditioning penetration in households was about 1% in 1990, and was almost at 100% in 2010 [10]. According to the International Energy Agency, cooling equivalent emissions were around 600 $MtCO_2$ in 1990; they have more than doubled in 2020, and the global energy demand from air conditioners is expected to triple by 2050 [11]. In Australia, even though households are equipped with air-conditioning, heatwaves have accounted for more deaths than all other natural hazards [12]. Given the increased cooling peak demand during heatwaves, the grid capacity is at risk and power shortages have happened in the past—and might occur again in the future [13–15]. In Europe, air conditioning has penetrated only 8% of households, but this number is growing fast: the number of units has doubled between 1996 and 2005 [9,10].

France has a temperate climate and, historically, buildings have included in their designs solutions to withstand cold winter temperatures. In the last fifty years, national building regulations have placed emphasis on high insulation and low airtightness to reduce heating needs and energy consumption. With the recent effects of climate change, the situation has already changed, as more French buildings tend to overheat during summers. Without appropriate mitigation and adaptation measures to climate change, people in buildings might be at risk in the near future [16–19]. Therefore, assessing the impact of warming temperatures on interior building conditions becomes a key challenge.

Countries have started to consider the already tangible effects of warming temperatures in their building regulations by using the most recent weather observations available for building weather files. In the U.S., the American Society of Heating, Refrigerating and Air-Conditioning Engineers (ASHRAE) is updating its climatic design conditions for Heating, Ventilation and Air Conditioning (HVAC) systems with the most recent climate observations ("2017", years 1990 to 2014) [20]. In the UK, the Chartered Institution of Building Services Engineers (CIBSE) provides typical reference years (TRY) with months selected from recent years as well (1984 to 2013). Additionally, design summer years are provided for overheating assessments. For instance in London, three design summer years (DSY) were selected from a moderate warm summer (1989), a short very intense warm spell (2003), and a long intense warm spell (1976) for three sites, considering, as well, the UHI effects [21]. Furthermore, the UK is, to date, the only country that provides, at a national level, future climate data from their UK Climate Projections 2009 (UKCP09) weather generator, available for overheating analysis of "buildings with long services life". In France, the typical reference year for the new Environmental Regulation (RE2020, starting in 2021) is made from weather observations from 2000 to 2018 [22]. For the last twenty years, the thermal regulation for buildings in France has been to ensure summertime indoor thermal comfort, with a mandatory overheating assessment on hot days for every new building (for which, in most cases, air conditioning was not needed in residential buildings). The next regulation will enforce this test with a month-long sequence containing observations of the 2003 heatwave. At present, overheating analyses are not systematic in most countries, even though they will most likely become more than necessary in the future. Robust weather files, possibly integrating future typical or extreme climate conditions, could be useful for the overheating assessment of buildings built today. Not accounting for future conditions at the design stage of buildings might result in future, recurring overheating periods

or peak cooling demands—which could have been prevented if buildings resilience to future warmer temperatures had been considered beforehand [23].

Consequently, there is a practical need for robust input future weather files for building energy modelling, considering climate change data are to be used by both researchers and building practitioners. However, in absence of a standardized approach or national regulations, there is a lack of knowledge about the tools and methods associated with reconstructing a future weather file from climate data. Which future scenario to choose? Which climate model? Which downscaling method? The uncertainties related to future climate projections and data are often not well known or understood by building practitioners. With the increase in the frequency of extreme temperatures [3,24], not only future typical weather files are needed, but future weather files, including consecutive hot days in the extremes of the distribution, such as extreme hot years or years containing heatwaves. These future weather files should help building practitioners at the design stage of the building to assess its capability to maintain or not maintain safe indoor temperatures under future climate without the use of air conditioning. In countries where air conditioning is already a common practice, these weather files could help to better size cooling systems.

This article proposes a methodology for assembling future climate data in order to provide ready-to-use future weather files for thermal building simulations from European Coordinated Regional Downscaling Experiment (EURO-CORDEX) multi-year climate datasets. A literature review on future climate data available today is first introduced (Section 2). Then, the methodology to convert the data into ready-to-use future weather files for building thermal simulations is detailed for both future typical weather years (TWY) and heatwave events (HWE) (Section 3). Finally, an example of the use of these future weather files to analyse indoor temperatures of a building case study in Paris is presented, using several climate models to consider uncertainties (Section 4).

2. State-of-the-Art Future Climate Data Available

2.1. Global Climate Models (GCMs)

The most sophisticated tool available today to represent climate simulations are coupled atmosphere–ocean general circulation models. These general circulation models, or global models, are driven by large-scale climatic forcings, such as the input of solar radiation, the concentration of greenhouse gases (outputs of the Representative Concentration Pathways, RCP), the distribution of oceans and continents, the presence of large continental surfaces such as mountains, etc. These models are spatially divided into a grid in which interactions between each cell of the grid are represented by physical equations. GCMs cover the entire globe, and their spatial resolution is quite coarse: At the time of the Intergovernmental Panel on Climate Change (IPCC) First Assessment Report (FAR), in 1990, their resolution was about 500 km, it has been about 100 km since the IPCC Fourth Assessment Report (AR4) in 2007. The representation of the relief, coastal, and ground occupation is sparse and, therefore, the resolution of these models is too high to be used for building thermal simulations. The full methodology of how climate change predictions are produced was summarized in [25]. Since the resolution of these models is too coarse, the climate community has undertaken data "downscaling" in order to realize local impact studies. According to Ouzeau, two distinct downscaling methods exist: statistical downscaling and dynamical downscaling [26]. An exhaustive and comprehensive review comparing the two methods was made by [27]. The two methods are presented in Sections 2.1 and 2.2.

Uncertainties in Global Climate Models

There are various uncertainties in global climate models. According to work of the authors Hawkins and Sutton, uncertainties can be sorted into three main categories [28,29]:

- The uncertainties related to the internal climate variability: these are natural fluctuations of climate from one year to another, or what is commonly called meteorology. For instance, from one

year to the next, the weather can be abnormally cold even though the tendency over ten years is a warming temperature.

- The uncertainties related to the climate model that is used from one climate model to another; predictions can vary greatly because the assumptions in the climate models can vary, or some climate aspects may be better represented in one model than another.
- The uncertainties related to the scenario that is considered: this is the uncertainty related to societal development, adaptation, and mitigation policies for climate change.

They compared model projections over the historical period 1955–2000 with observations and showed that the observations laid within the uncertainty range (Figure 1). They also showed that with time, the uncertainty in temperature predictions becomes increasingly higher. At the end of the century, depending on the natural variability of climate, on the climate model, and on the socio-economic scenario considered the average global temperature, it is expected to increase from +1.2 °C to +4 °C. Furthermore, depending on the time-period, the uncertainties from the three categories are not always the same. At the beginning of the century, the uncertainty related to the internal climate variability is high in comparison to the other uncertainties, but should become less significant with time. In the middle of the century, the uncertainty related to the climate model is the most significant; whereas, towards the end of the century, the uncertainty related to the scenario is the most important one, even though the uncertainty related to the climate model is still quite significant. In the article, the authors also mention that the period around 2050 is when temperature predictions will be best when compared with other periods during the century [28,29].

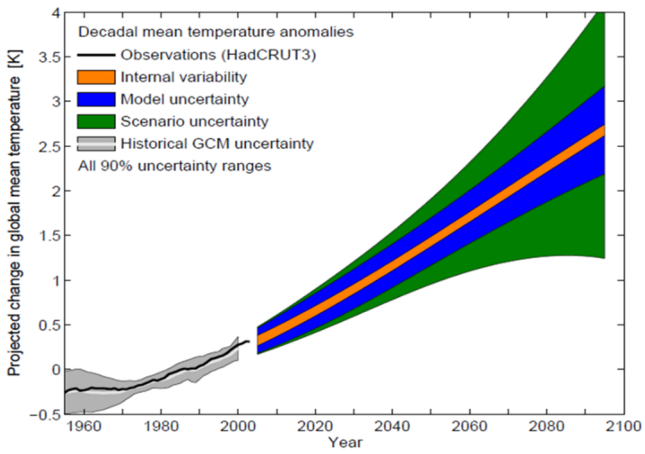

Figure 1. Uncertainty in average temperature decanal projections during the 21st century from global climate models (GCMs), part of the CMIP3 project: uncertainty related to the climate internal variability (orange), model uncertainty (blue), and scenario uncertainty (green). Projections are calculated compared to the period 1971–2000. Historical uncertainty (grey), models average historical (white), observations (black). Reprint with permission [29]; 2020, Springer Nature.

2.2. Statistical Downscaling

2.2.1. The Morphing Method

Beyond several statistical downscaling methods, the one most widely used for building simulations is the morphing method, developed by Belcher et al. in the United Kingdom [30]. This method was used by the CIBSE in 2008, who produced future morphed typical weather test reference years (TRY) and design summer years (DSY), two weather files ready to be used for building simulations. The principle is that from an existing weather file under present day climate (for instance, a typical weather file), a morphing equation is applied to each variable x_{0h}. Three types of possible equations «shift», «stretch», or a combination of shift and stretch are used to calculate each future climate variable

x_h. The climate change aspect, issued from one or several GCMs, is integrated through Δx_m and α_m, which are respectively the monthly average and monthly average daily range of the climate variable. In the equation shift and stretch, x_{0m} is the monthly mean value of the climate variable.

Morphing equation "shift":

$$x_h = x_{0h} + \Delta x_m \quad (1)$$

Morphing equation "stretch":

$$x_h = \alpha_m \times x_{0h} \quad (2)$$

Morphing equation "shift and stretch":

$$x_h = x_{0h} + \Delta x_m + \alpha_m \times (x_{0h} - x_{0m}) \quad (3)$$

The equation shift is used for variables who evolve with an absolute change in average, such as the atmospheric pressure. The stretch equation is used to represent a coefficient change in the average or in the variance, such as the wind speed. It is also used if the climate variable needs to be set to zero (for instance the solar radiation during the night). Finally, the equation shift and stretch combination is used to represent both a change in average and standard deviation. For example, it was used for the dry-bulb temperature to represent a change in average, minimal and maximal temperatures. The morphing equations for most climate variables are described in [30].

The morphing method has been implemented in the Climate Change World Weather Generator (CCWWeatherGen), an online free Excel tool created by the Sustainable Energy Research Group from the University of Southampton. The tool allows to convert a reference weather climate file to a future climate change weather file, both in Energy Plus Weather (EPW) format. This format was specifically chosen to make the data easily available for building simulations. The methodology of the CCWWeatherGen was described in [31]. The tool is based on data generated by the GCM HadCM3, following the A2 socio-economic scenario. The authors chose to use GCM data in order to increase the tool's accessibility to a large number of countries. The HadCM3 climate model was compared to 29 other climate models and was chosen because, at the time, it was the only model that had all necessary climate variables for morphing and recreating a ready-to-use weather file [32]. The tool allows users to recreate future weather files on three future periods: 2011–2040, 2041–2070, and 2071–2100. The details of the morphing equations for each variable used by the generator were described in the technical reference manual for the CCWWeatherGen [33]. Some of these equations have been revised in [31]. Even though the tool is very practical to generate future weather files, it has a number of drawbacks and uncertainties detailed in Section 2.2.3.

The morphing method has also been implemented in the Weather File Module of the WeatherShift commercial tool, developed by Arup and Argos Analytics. They used future climate data from 14 GCMs used for the IPCC Fifth Assessment Report (AR5), and it is possible to access future climate data on three future periods: 2026–2045, 2056–2075, and 2081–2100 from the reference period 1976–2005 under the scenarios RCP 4.5 and 8.5. The morphing method is applied to eight climate variables from typical weather files: the mean, maximum, and minimum daily temperatures, the relative humidity, the daily total solar irradiance, the wind speed, the atmospheric pressure, and the precipitations. Cumulative distribution functions (CDF) are created via interpolation between the monthly means from each climate model [34]. This method allows for consideration of the uncertainty related to each climate model and the user can select the percentile value of the CDF when selecting the future weather file. Moazami et al. compared future climate predictions from the CCWWeatherGen and WeatherShift [35], and concluded that WeatherShift presents a major drawback by modifying only a few climate variables beyond those having an important impact on buildings, such as the global solar radiation However, WeatherShift allows for comparing outputs from different climate models and, therefore, assessing climate model uncertainties, which the CCWWeatherGen cannot [36].

2.2.2. Stochastic Weather Generators

Weather Generators can also be used to recreate future stochastic weather files. For instance, the software Meteonorm also proposes ready-to-use future climate weather files, under three IPCC future scenarios (B1, A1B, and A2 from AR4) and for several ten-year future periods from 2010 until 2100. It is based on a stochastic method, which consists of applying statistics to a set of climate data observations. The future generated climate data are an "average" of data issued from the 18 climate models used during the AR4. Only three climate variables are modified during the generation of future weather files: the temperature, the solar radiation, and the precipitations [37].

Similar to the morphing method, climate change projections are integrated in a monthly average and applied to the present data. In England, a weather generator (WG) was developed along with the UK Climate Projections 2009 (UKCP09). This generator is a stochastic model, allowing it to produce future probabilistic years and future extreme years at an exceptional grid of 2 km [38]. Future years can be generated for thirty-year periods every ten years, from 2010 until 2100, under three future emission scenarios (high, medium, low). Data were calibrated against observations and eleven RCM projections, allowing to reproduce future probabilistic projections through a vast number of future weather files. These projections are used today in the UK for studying indoor conditions in buildings under climate change [39].

2.2.3. Uncertainties in Statistical Downscaling

Uncertainties related to the spatial scale lay in the statistical downscaling method. GCMs data are from a 100 km grid; whereas, the spatial scale of the observed weather data used to reconstitute the future EPW is much smaller. Uncertainties related to the time factor also need to be considered, since climate change variations are integrated through monthly averages. Information is hidden in these monthly averages, such as daily variations and temperature extreme events (e.g., heatwaves). Jentsch et al. compared morphed data from the GCM HadCM3 and dynamically downscaled data from the RCM HadRM3, which was generated from the GCM HadCM3. They concluded that, despite a good correlation in the average variations, the morphed data could not accurately represent climate extremes such as heatwaves or cold spells [31]. The authors of the morphing method also mention uncertainties in the equations themselves, since climate variables vary independently from each other. Other uncertainties are the uncertainties related to the climate model and to the scenario chosen. While the WeatherShift tool allows to both select through CDF a percentage (%) of future predictions beyond the climate models, and to choose between two future socio-economic scenarios, the CCWWeatherGen only predicts future climate data based on one climate model (HadCM3) and one future socio-economic scenario (A2, equivalent to RCP 8.5). Therefore, to this latter, neither uncertainties related to the scenario nor to the climate model can be assessed. The CCWWeatherGen has been widely used in recent building simulation studies because it is free to access and easy-to-use. Unfortunately, none of these studies mentioned the impact of the uncertainties on their results. Moreover, some authors directly applied the morphing technique to multiple GCMs for building simulations; thus, considering model uncertainties [40,41]. However, systematically considering model uncertainties for building simulations is not yet a practice in the building research community. Despite the uncertainties related to this method, statistically downscaled future weather files are the ones largely used by the building research community, as they are the easiest and most available methods.

2.3. Dynamical Downscaling (Regional Climate Models)

Regional climate models (RCMs) are climate models issued from global climate models with a smaller spatial resolution (10 to 50 km). They are "dynamically downscaled" by the climate research community. Since only a specific part of the world is represented in a RCM (usually a continent or a portion of a continent), the grid has a higher spatial resolution, allowing better representation of local climate effects. The regional climate models use meteorological boundary conditions (temperature,

water vapour and cloud variables, wind speed, etc.) from global climate models. Each RCM is downscaled from one GCM, but the same RCM can be downscaled from other GCMs as well, resulting in various GCM_RCM combinations. RCMs allow simulations of climate phenomena that happens on a smaller scale, such as the state of the atmosphere (precipitations, storms, etc.), the physical representation of the complex land topography and coastline, the surface vegetation distribution, the inland bodies of water, the land occupation including urban settlements, etc. Oceanic characteristics are not modelled (they are boundary conditions); the RCMs only model the atmosphere and the vegetation. RCMs also have a refined time resolution, allowing them to better represent extreme events. Using RCMs is necessary for local adaptation studies. Regional climate modelling originated in the late 1980s and the European community has been very active in RCM development. RCMs allow to represent extreme events, both spatially and temporally. Giorgi compared the total precipitation above the 95th percentile over the Alpine region in Europe projections of a GCM, a RCM and observations (Figure 2). He could conclude that it is obvious that RCMs allow to represent with a greater accuracy both the spatial and temporal complexity of the observed extreme precipitations. Moreover, RCMs have proven to well represent spatially other extreme events, such as heatwaves [4,42–44].

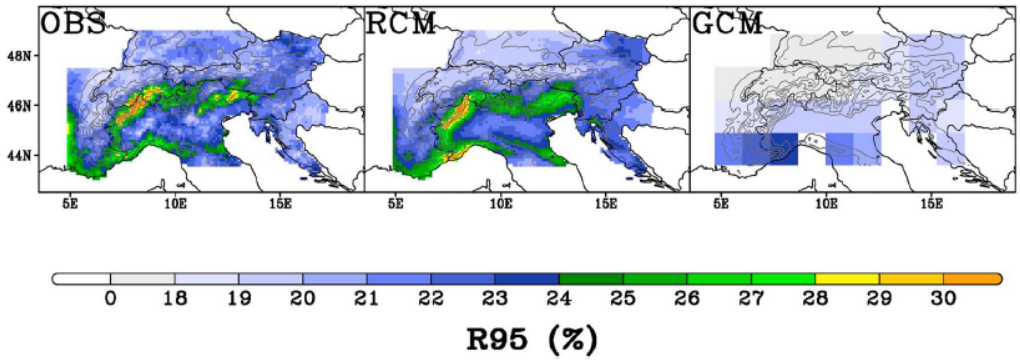

Figure 2. Fraction of total precipitation above the 95th percentile (R95) over the Alpine region. Units are in percent of total precipitation and the simulation period is 1975–2004. OBS = observations, RCM = regional climate model, GCM = global climate model; Adapted from [45].

2.3.1. EURO-CORDEX Climate Data

Several projects initiated by the World Climate Research Program (WCRP) allowed to improve the accuracy of regional climate models. As inconsistencies were noticed along regional climate models, these projects allowed to establish a common simulation protocol among climate laboratories. The model's resolution was improved to ~25 km through the PRUDENCE & ENSEMBLES projects [1,2]. Today, a resolution of an unprecedented resolution of ~12 km is available for the models that are part of the European Coordinated Regional Downscaling Experiment (EURO-CORDEX) [46]. EURO-CORDEX is today the main reference framework for regional downscaling research [47]. Its main goals are to evaluate and improve the different RCMs via a better understanding of regional and local climate phenomena and uncertainties and to foster communication and knowledge exchange among the climate community. The project also aims to generate and maintain a consistent database of downscaled multi-year projections over regions worldwide that can be used for adaptation studies in various sectors, such as agriculture, fire risk, air quality, or heat stress [45]. These data can be used by the building sector and this article will show a demonstration of this. A large amount of RCM data is available on the CORDEX project platform [48]. The platform is updated regularly, and new climate data are uploaded often. CORDEX domains are available for all parts of the globe (Figure 3). EURO-CORDEX projections are available for Europe, on a grid resolution of 12.5 km; CORDEX projections are available at a 25 km grid resolution in the Middle East and in North Africa and about 50 km in the rest of the world. Data are available at the multi-year format on different time scales: monthly, daily, every six hours and three hours, during the historical period from 1976 to 2005 and for the future period, from 2006 to

2100. Depending on the model, data are available for the RCP 4.5 and or RCP 8.5 scenarios. At the three-hour time step, all necessary climate data to reconstruct a weather file for building simulations are available. At larger time steps, more climatic variables are available. The detail of the available climate data is described in [49]. For some models and climate variables, some bias-adjusted data are available. However, a large part of the data available on the platform has not been bias-adjusted.

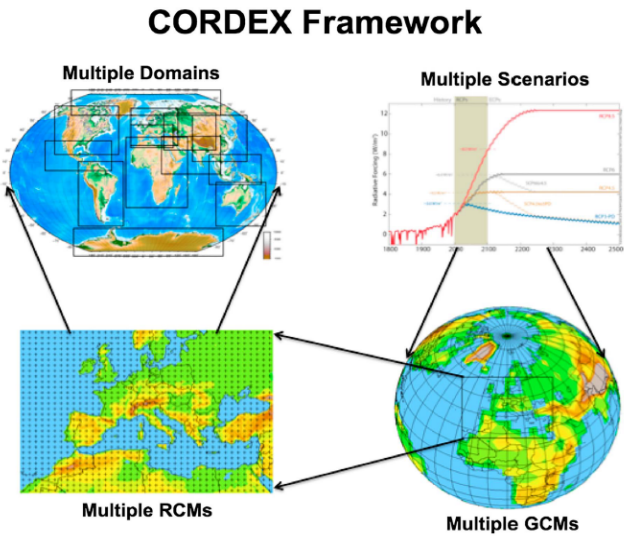

Figure 3. Representation of the Coordinated Regional Downscaling Experiment (CORDEX) Framework. Reprint with permission [45]; 2020, John Wiley and Sons.

The main inconvenience of these data is that—as of the date of this article—most of them are only available every 3 h. For building simulations, interpolations need to be made to downscale to the 1 h format, which increases the complexity of the process. For some climate variables, data are not instantaneous but averages, which makes it difficult to reconstruct a weather file at the 1 h time step. However, hourly data have been recently uploaded on the platform, so there are good chances that data at that time step will be available in the future. For each climate variable, one file is available in Network Common Data Form (NetCDF) format on the entire spatial grid of the RCM. Therefore, formatting and storage are required in the process of reconstructing future weather files ready to be used in building simulations. The advantage of the CORDEX project is that it provides a lot of data from different models and different scenarios for everywhere in the world, allowing impact studies considering models and scenarios uncertainties. Moreover, future climate data are available on a multi-year format from 2005 until 2100; therefore, extremes of the distribution on different timescales can be investigated. EURO-CORDEX multi-year projections are also available on the French DRIAS platform [3], dedicated to adaptation studies. However, data on this platform are daily averages, which do not fit the time-step required for dynamic building simulations. According to Moazami et al., who conducted a review on scientific papers assessing the impact of climate change on building performances, only 10% of the articles reviewed used dynamical downscaling [50]. This might be because regional climate data have only very recently become easily accessible. Indeed, only a few articles use RCM data for building thermal simulations [51].

2.3.2. Uncertainties in Regional Climate Models

According to Giorgi, in the last generations of GCMs the range of temperature difference between the models remains fairly high, from 1.5 °C to 4.5 °C which is in accordance with Hawkins et Sutton [45]. These differences are due to the hypothesis laying behind the models, such as their representation of different climate feedbacks (sea ice albedo, water vapour, and cloud–climate). Model uncertainty increases when downscaling from global scale to regional scale, and the regional temperatures from

various models can vary from 3 °C up to 10 °C, with the highest differences found in northern high latitude regions. In an older article, Giorgi assessed the uncertainty from GCM and RCM separately of temperature and precipitations in Europe, both in summer and winter (Figure 4). Regarding the summer temperature, he showed that the highest uncertainties were the one related to the scenario and the GCM, followed by the uncertainty related to the RCM. Only a small part of the uncertainty was related to the internal climate variability. By summing the uncertainty related to RCM and GCM, it appears that the model uncertainty becomes higher than the uncertainty due to the scenario. In order to assess the impact of these uncertainties on the results, it is necessary to conduct simulations with climate predictions from various climate models and socio-economic scenarios. According to Giorgio, for impact assessment studies, it is necessary to use well-designed scenario-GCM_RCM matrices to fully assess the uncertainties associated with regional and local climate change information [45]. Since numerous climate data are available on the CORDEX platform, it is possible to assess the climate data uncertainty by using multiple future climate files for building simulations. In the literature, most authors are generally using one climate model to assess future temperatures, sometimes with two socio-economic scenarios under different future periods. This can be explained by the fact that up until very recent years, future climate data from regional climate models were hard to find. To the authors' knowledge, only few researchers have considered regional climate model uncertainties by comparing the temperature outputs from three climate models and their impact on building thermal simulations [50].

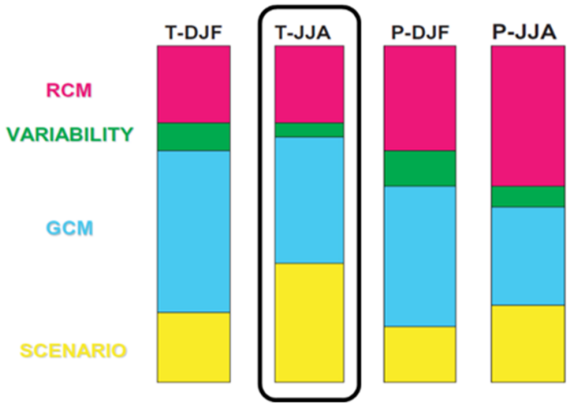

Figure 4. Relative contribution to the uncertainty in the simulation of climate change over Europe originating from various sources: RCMs (8 models), internal variability of GCMs, GCMs (4 models), scenarios (2 used). T is the temperature and P is the precipitation. DJF is winter and JJA is summer. The highlighted column is the summer temperature. Reprint with permission [52]; 2020, EDP Sciences.

2.3.3. Data Bias in Regional Climate Data

The bias is the difference between the projected values from the model and the observations. The raw outputs from the regional climate models are not bias adjusted and, therefore, need to be post processed to consider bias correction. Bias-adjusted values of different climate variables are not expected to match exactly with the observations, as they do not represent day-to-day evolution of the weather. However, using the raw output data from climate models during the historical period and during the future period allows comparisons, not in absolute values, but in relative values. In articles from authors using data from regional climate models for building thermal simulations, sometimes the question of the bias is not addressed; therefore, it is hard to know if it was considered or not. Thus, when using regional climate data, one should be aware if the data were bias-adjusted or not. Different techniques exist to correct the model bias, commonly called "bias-adjustment" methods. Usually, by comparing the raw-data output during the reference period with the measurements, it is possible to calculate a correction factor. This correction factor itself is applied both to the historical climate (historical-bias-adjusted) and to the future climate (future-bias-adjusted). The bias-adjustment

methods allow correcting all the climate variables distribution functions; they not only correct the average values, but also the extremes of the distribution curve by comparing them to observations. Some methods are the distribution-based scaling method (used by the Swedish Meteorological Hydrological Institute, SMHI), the quantile mapping method (used by the Norwegian Meteorological Institute (METNO) or the cumulative distribution function method (used by the Pierre Simon Laplace Institute (IPSL)). The main assumption is that the correction factor (difference between the model predictions and the reality) does not change with the changing climate and, therefore, the bias will be the same in the future. However, it is not known if the model bias will change in the future or not, adding a supplementary uncertainty.

2.4. Comparison of the Downscaling Methods

This section has described the two different downscaling methods that exist, and Table 1 presents the main advantages and disadvantages of each method.

Table 1. Advantages and disadvantages of downscaling methods [16,31,50,53].

	Statistical (Morphing, Stochastic)	**Dynamical (Regional Climate Models)**
Advantages	Simple method Low computational power Energy Plus Weather (EPW) files (future typical years) ready to use for building simulations	Physically consistent datasets across different weather variables Extreme events (such as heatwaves) are well represented
Disadvantages	Climate change is only represented through monthly averages Lack of physical consistency between weather variables Future extreme events are not represented Models and scenarios used depend on the tool, which makes it difficult to assess uncertainties Analogies to present-day climate, assumptions that future weather patterns will be similar to present-day observations	High storage capacity needed All data needed to reconstruct a weather file not available at the hourly format yet on the CORDEX platform (3 h time-step data available) Formatting and interpolations are required to reconstruct an EPW file (time-consuming and requires some knowledge) Most data on the CORDEX platform are not bias-adjusted

2.5. Future Weather Files Containing Temperature Extremes

Most authors using future climate data to assess the impact of climate change on building thermal simulations are using future typical weather years. In fact, this underestimates climate change effects, since temperature extremes are increasing faster than temperature means [54], which has been proven recently with multiple heatwave occurrences [55]. On a risk point of view, it is crucial to evaluate indoor building conditions under future hot temperatures, when the population is most at risk. Assessing the resilience of buildings to future climate with future weather files containing warm years, extreme hot years, or heatwaves, is a very recent practice. According to Moazami et al., out of 34% of the authors who have used extreme conditions, half of the papers are from the United Kingdom, where future extreme weather files are available at a national level from the stochastic Weather Generator [50]. Therefore, if future data containing extremes were available at the national level in France, there is a chance that these would be highly used in climate change impact studies for building simulations.

Despite the lack of future weather files containing temperatures extremes, some authors have been using recorded hot years or heatwave observed data to assess the resilience of the building to hot external temperatures [56–58]. Others have developed methodologies to reconstitute future weather files containing temperature extremes, such as Nik, who used data from regional climate models to reconstitute future extreme hot years, selected from a centile of the dry-bulb temperature [59].

Ramon et al. suggested the use of future multi-year datasets to assess the resilience in extreme weather conditions, and recreated several typical and extreme year methods for comparison [60]. In the UK, Liu used the UKCP09 British weather generator to generate future probabilistic hot summer years and, more recently, future hot event probabilistic years [61,62]. Jentsch et al. developed near-extreme summer reference years (SRY) for the United Kingdom, adapting the UK design reference years (DSY) by adding the solar radiation and cloud cover in the selection process to better represent typical outdoor conditions for buildings overheating (high temperature, high solar radiation, and low cloud cover) [63,64].

To the authors' knowledge, reconstituting weather files containing future heatwaves to assess the resilience of buildings during a hot event has only been done by [62]. However, stochastic data are not available in France. Many authors have characterised the occurrence, frequency, and duration of future heatwaves in the climate research community; however, little of this research has been used by the building research community. In France, the National Center for Meteorological Research (CNRM)and IPSL laboratories are conducting research on future climate data and are particularly active in future climate data research. Lemonsu et al. characterised and identified future heatwaves from different Representative Concentration Pathway (RCP) scenarios, and climate models under both historical and future scenarios, and used these future heatwaves to assess different mitigation and adaptation scenarios at the urban level [65,66], but not at the building scale. More recently, Ouzeau et al. developed a method to detect future heatwaves from a climatological point of view from a EURO-CORDEX dataset [67]. In this study, we used this method to detect future heatwaves in EURO-CORDEX ensemble multi-year projections to build future climate files containing heatwaves to be used by building practitioners. Since the projections are available for many locations worldwide, this methodology can be used for other countries than France using the CORDEX data for outside of Europe.

2.6. Uncertainties Propagation from Climate Projections to Future Weather Files

In the climate community, it is advised to do impact assessments with several climate models, if not all, to quantify uncertainties. However, in the building community, many articles display results for one climate model and assess the effects of climate change in absolute future temperatures. Most authors do not mention model biases and only a few consider uncertainties by comparing several climate models and socio-economic scenarios [68]. Figure 5 summarizes the different methods and tools used to reconstruct future weather files from multi-years climate projections, and the uncertainties propagation along the modelling chain.

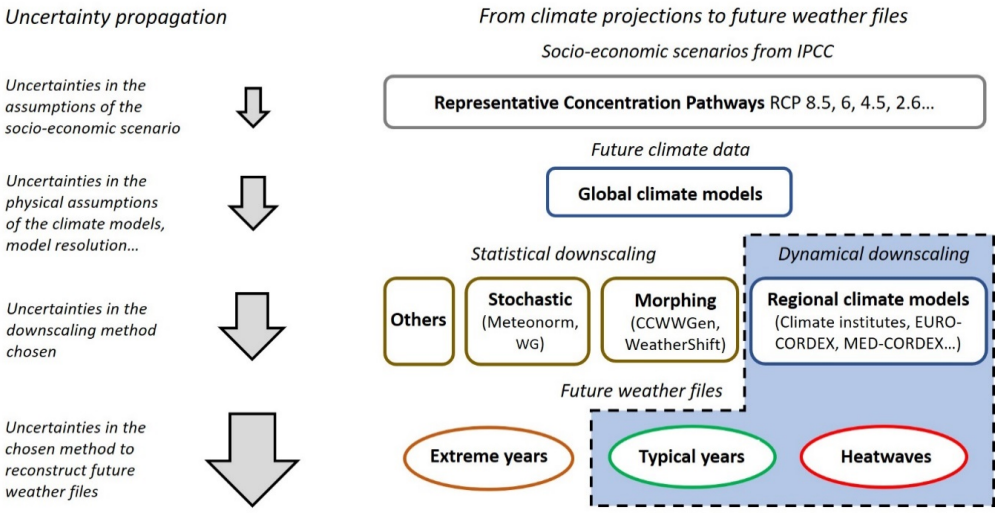

Figure 5. Uncertainty propagation along the modelling chain from multi-years climate projections to future weather files. IPCC: Intergovernmental Panel on Climate Change.

3. Methodology for Assembling Future Weather Files

In this section, we describe the methodology proposed to assemble future weather files from the CORDEX climate multi-year projections. Two future weather files are provided: future typical years (TWY) and future heatwave events (HWE). Figure 6 displays a summary on the reconstruction of the future weather files.

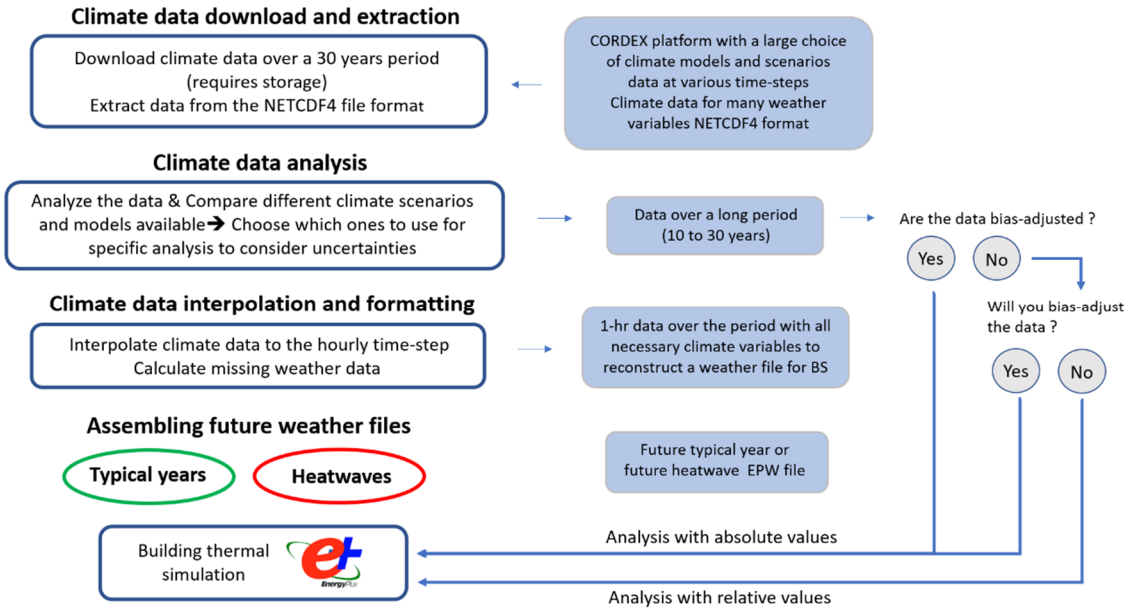

Figure 6. Methodology for assembling future weather files from CORDEX climate data.

3.1. Climate Data Download and Extraction from the CORDEX Platform

It is possible to access the CORDEX simulations from different entry points, through the Earth System Grid Federation (ESGF). We used the one from the IPSL laboratory: ESGF-NODE.IPSL.UPMC.FR [69]. We analysed which models could provide the necessary climate variables to reconstruct a weather file for at least one future RCP scenario (dry-bulb temperature, absolute or relative humidity, solar radiation, cloud cover, atmospheric pressure, and wind speed). In November 2019, data for these six weather variables were available every three hours for the regional climate models presented on Table 2. Data from six models were uploaded in 2018 and for five additional models in 2019. Some data are available on the hourly time-step, but not for all of the six necessary weather variables. The data are available under the NetCDF4 format, largely used by the climate community. Each file contains all the grid of one CORDEX domain (Figure 3). We downloaded data for the Europe domain on a 0.11° grid, in rotative coordinates (equivalent to a 12.5 km grid). The architecture of the NetCDF4 files is explained in the CORDEX Archive Design document [70]. We extracted the data for Paris, our case-study city, through a Python code, allowing to find the closest data point on the grid to a given set of latitude and longitude.

Table 2. Climate models for which the six climate variables (dry-bulb temperature, specific humidity, atmospheric pressure, global horizontal radiation, cloud cover, and wind speed) are available on the CORDEX platform [69] at the 3-h time step on the Europe domain (12.5 km grid) for historical and future periods. The table was updated on 6 November 2019.

Institution	Driving GCM	CMIP5 Ensemble Member	RCM_VersionID	Date Uploaded on the CORDEX Platform	GCM_RCM Combination Short-Name
SMHI (1)	CNRM-CERFACS-CNRM-CM5	r1i1p1	RCA4_v1	2018-02-26	CNRM_RCA
CNRM (2)	CNRM-CERFACS-CNRM-CM5	r1i1p1	ALADIN63_v2	2019-04-19	CNRM_ALADIN
SMHI	NorESM1-M	r1i1p1	RCA4_v1	2018-08-20	NorESM_RCA
SMHI	MPI-M-MPI-ESM-LR (5)	r1i1p1	RCA4_v1	2018-02-26	MPI_RCA
GERICS (3)	MPI-M-MPI-ESM-LR	r3i1p1	REMO2015_v1	2019-09-25	MPI_REMO
ITCP (4)	MPI-M-MPI-ESM-LR	r1i1p1	RegCM4-6_v1	2019-05-02	MPI_RegCM
SMHI	ICHEC-EC-EARTH	r12i1p1	RCA4_v1	2018-02-26	EC-EARTH_RCA
SMHI	IPSL-IPSL-CM5A-MR	r1i1p1	RCA4_v1	2018-02-26	IPSL_RCA
SMHI	MOHC-HadGEM2-ES	r1i1p1	RCA4_v1	2018-02-26	HadGEM_RCA
SMHI	MOHC-HadGEM2-ES	r1i1p1	ALADIN63_v1	2019-10-04	HadGEM_ALADIN
SMHI	MOHC-HadGEM2-ES	r1i1p1	RegCM4-6_v1	2019-05-02	HadGEM_RegCM

(1) Swedish Meteorological Hydrological Institute (SMHI); (2) National Centre for Meteorological Research (CNRM); (3) Climate Service Center Germany (GERICS); (4) International Center for Theoretical Physics (ITCP).

3.2. Analysis of Climate Data Available on the CORDEX Platform

We analysed the temperatures over the historical and future periods 1976–2005 and 2041–2070; considering a thirty-year period is standard in climatology to eliminate the uncertainty related to the internal climate variability. This historical period is mostly used in the literature and the least reference period available on the platform. In the literature, even though there are slight differences among tools and methods, it is generally accepted that the 21st century can be divided in three future periods: The short-future (2011–2040), medium-future (2041–2070), and long-future (2071–2100).

In France, since the lifetime of a building is between 50 and 100 years, we considered 2041–2070 as a key period during the building operation. Since most research papers, both in the climate and in the building research community, have put more emphasis on studying the short- and long-term future, we found it interesting to study an intermediate period. Moreover, while the effects of climate change will become more predominant, with more intense and long heatwaves in the second part of the century, their uncertainty will increase as well [5]. We considered it important to study the second part of the century, while focusing on the first part to reduce uncertainty.

We compared dry-bulb temperature predictions from 11 climate models and the two socio-economic scenarios RCP 4.5 and 8.5. The statistical distribution of the monthly average temperatures of July and August over the historical and future periods is presented on Figure 7. Each boxplot represents July and August monthly temperatures over 30 years (sixty data points per boxplot) from one climate model. For each climate model, one boxplot is displayed for the reference period, and one or two boxplots for the future, depending on data's availability. Maximum and minimum monthly mean temperature values are at the whiskers as long as they are within the 1.5 interquartile range (IQR) of the upper quartile and lower quartile respectively, otherwise, they are outliers, displayed as black diamonds. The green triangles represent the average temperatures. Temperature predictions vary greatly from one climate model to another: Comparing the lowest temperatures median to the highest for the RCP 8.5, there is a difference of 7 °C along with the models. As data from Figure 7 were not bias-adjusted, it is preferred to compare the future predictions to the historical predictions from one climate model and quantify the temperature increase rather than absolute values. This is also recommended as a preferred method by climatologists to minimize the model biases [71]. For this purpose, for each model, the average temperature increase between the historical period and the future period for the scenario RCP 8.5 over the thirty years is written. Models can be distinguished in two groups: the ones with the lowest increase in average (from +1.4 °C to

+2.3 °C) and the ones with a higher increase, (from +2.8 °C to +3.4 °C). These groups are formed from the GCMs and not the RCMs, as all RCMs downscaled from CNRM and Max Planck Institute Earth System Model (MPI-M-MPI-ESM-LR, MPI used from here) are in the first group, whereas the models downscaled from the Hadley Centre Global Environment Model (MOHC-HadGEM2-ES, HadGEM used from here) are in the second group. The RCM probably makes a difference in the extremes of the temperature distributions, which are not shown here since Figure 7 only displays monthly averages. The higher absolute temperatures (over both the historical and future periods) are from any GCM with the RCM Regional Climate Model RegCM4, or from any RCM with the GCM HadGEM, which is confirmed, since the temperatures from the combination HadGEM_RegCM4 are the highest. Finally, temperature values differ more along the climate models than between the two RCP scenarios, which confirms the uncertainty related to climate models is higher than the one related to the concentration pathways for the considered future period 2041–2070. We pursue the analysis with the Rossby Centre regional Atmospheric climate model (RCA) downscaled from 3 GCMs under the future RCP 8.5 scenario: HadGEM_RCA (8/11 model in absolute future average temperatures and high mean temperature increase of 2.8 °C between historical and future period), IPSL_RCA (7/11 model in absolute future average temperatures and highest mean temperature increase of 3.3 °C between historical and future period) [72] and MPI_RCA (2/11 model in absolute future average temperature, and average mean temperature increase of 2.2 °C between the historical and future period).

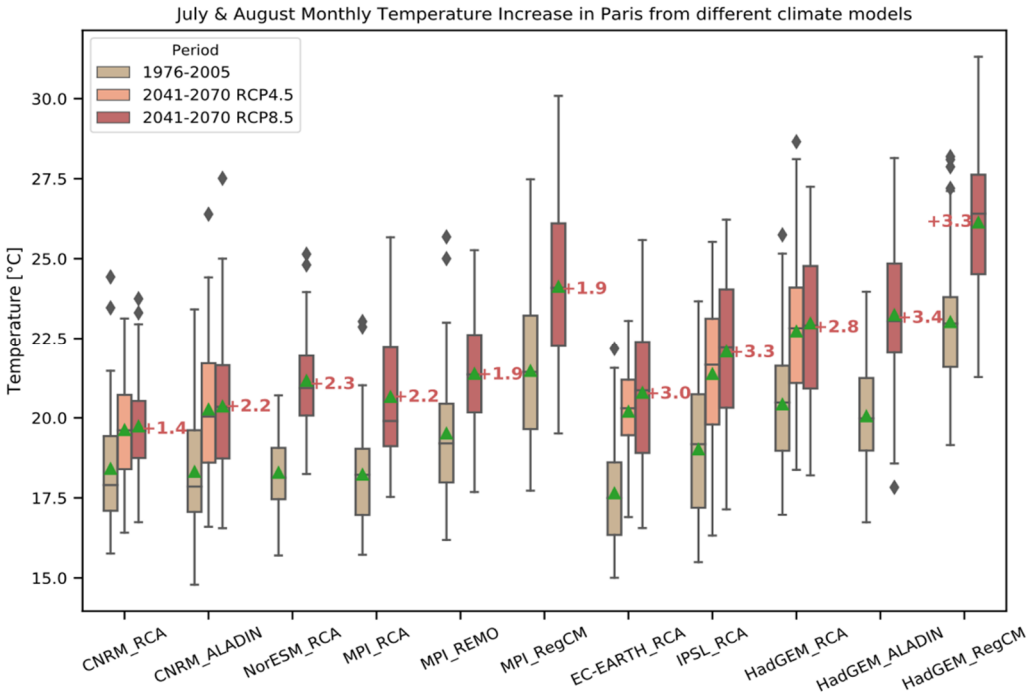

Figure 7. Statistical distribution of monthly average summer (June, July, August, and September) temperatures in Paris over the reference period 1976–2005 and the future period 2041–2070, under the socio-economic scenarios Representative Concentration Pathways (RCP) 4.5 and RCP 8.5 from different climate models (downscaled RCM identified as GCM_RCM).

In order to investigate temperature extremes as well, we analysed the temperature every three hours over the historical and future (scenario RCP 8.5) periods for the three climate models (Figure 8) curve, consisting of temperatures for the months of July and August, every three hours, over thirty years (14,880 data points). Bias-adjusted data are plotted for comparison with the raw-output climate data. On the CORDEX platform, in 2019, bias-adjusted data were available on a 3 h time step for the climate variables dry-bulb temperature, global horizontal radiation, and wind speed. They were bias-adjusted by the IPSL laboratory with the method described in [73]. Since bias-adjusted data are

not available for the other necessary climate variables to reconstruct a future weather file, for the rest of the analysis we used the raw-output climate data. Additional bias-adjusted climate data will be uploaded on the CORDEX platform according to the EURO-CORDEX guidelines [74]. From Figure 8, for all models, bias-adjusted temperatures are warmer than the raw-climate output, except for the warmest temperatures of the model HadGEM_RCA (model with the highest absolute temperature values). IPSL_RCA bias-adjusted temperatures are closer to their respective raw-output temperatures than MPI_RCA, both during the historical and future periods, which suggests an underestimation of temperatures by this model during the July and August months. HadGEM_RCA bias-adjusted temperatures are close to the raw-output until 20 °C, but for higher temperatures, the difference increases and bias-adjusted temperatures are finally lower than the raw-output. At 50% of the distribution, during the historical period, all bias-adjusted temperatures are about 20.0 °C whereas the raw-outputs temperatures are about 17.7 °C, 18.4 °C and 19.7 °C for MPI_RCA, IPSL_RCA, and HadGEM_RCA, respectively. It was expected that all bias-adjusted temperatures over the historical period would be similar since they are the raw-outputs temperatures corrected with the historical observations. During the future period, at the 50% centile of the distribution, the bias-adjusted temperatures are higher, for all models, than the raw-output temperatures (22.3 °C, 23.0 °C and 22.2 °C for MPI_RCA, IPSL_RCA, and HadGEM_RCA, respectively versus 20.0 °C, 21.4 °C, and 22.0 °C). Regarding the end of the distribution tail, at the 95% centile (Figure 8 bottom), the bias-adjusted temperatures during the future period are higher for the models MPI_RCA and IPSL_RCA (32.7 °C and 33.1 °C versus 30.4 °C and 32.5 °C, respectively) but lower for the model HadGEM_RCA (31.8 °C versus 33.9 °C). In all cases, temperature differences along models are smaller for the bias-adjusted data than the raw-output ones, suggesting that using bias-adjusted data reduces model uncertainty. However, using bias-adjusted data also increases uncertainties since most methods assume that the bias correction factor will not change with time, which is, in fact, not known. At the end of the distribution tail (1) for all models, and over both the historical and future periods, raw-output and bias-adjusted temperatures are sensitively very close.

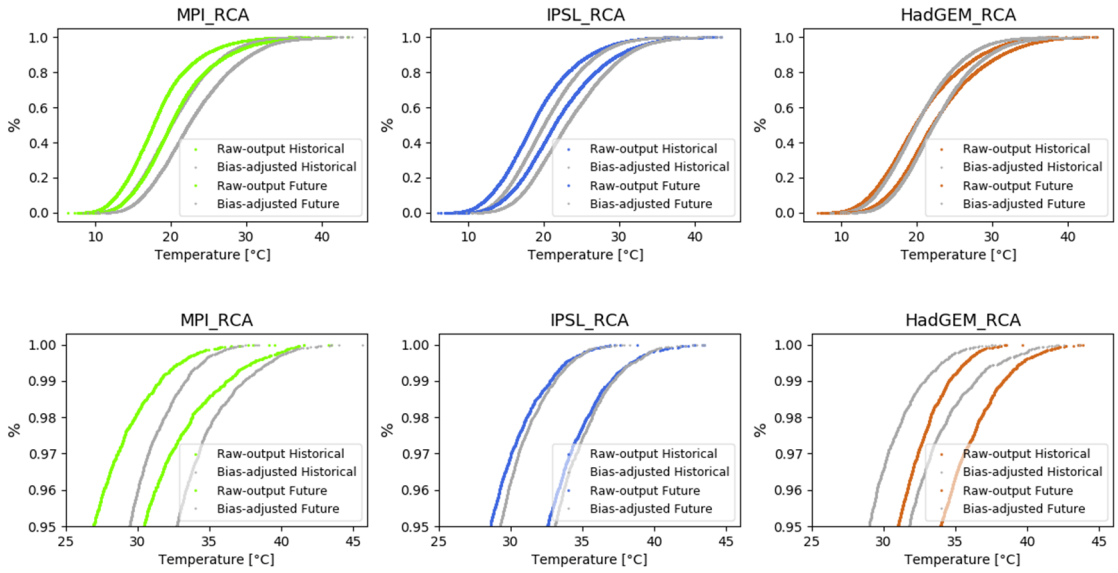

Figure 8. Comparison of temperatures, data every 3 h over the historical and future periods, for the three climate models, raw outputs vs. bias-adjusted. Top: All data points, Bottom: Zoom over the 0.95 to 1 centile.

Since all climate variables (needed to reconstruct future weather files) are not bias-adjusted on the CORDEX platform, we will use the raw climate data. This way, we can quantify for each model the temperature increase by the difference between the future and historical temperatures.

Table 3 summarizes the temperature increase for each model at the 0.5 centile and at the end of the distribution tail (0.95 and 0.99) between the historical and future periods (2041–2070) for the three climate models. The increase at the 0.5 centile is in accordance with the findings of [75], which predict, in France, a mean increase of +2.1 °C in the near future and of +4.5 °C in the long-term future. The end of the distribution tail increase is as important as the medium one, since it is when extreme events happen. Heatwaves will be found during these temperatures, and the temperature at a high percentile is also the one used for the design-day of cooling systems. Depending on the standards, methods to choose the design-day differ, and the percentile can be between 0.90, 0.95, and 0.99 [76,77]. They usually analyse datasets with hourly data points; the one we considered has data points every three hours, at 12 am, 3 pm, and 6 pm; therefore, the temperature peak might be missed. From Table 3, it is noticeable that the temperature extremes have a higher increase than the temperature median, and for each model. Moreover, the uncertainty among the three climate models is lowest at the very end of the distribution tail (0.99).

Table 3. Temperature increase for the three climate models for the 0.5, 0.95, and 0.99 centiles of the temperature distribution between the future and historical periods relative to each analysed climate model.

Centile	MPI_RCA	IPSL_RCA	HadGEM_RCA	Uncertainty of Temperature Increase
0.5 centile (7440 h)	+2.3 °C	+3.0 °C	+2.3 °C	23%
0.95 centile (744 h)	+3.5 °C	+4.1 °C	+2.9 °C	29%
0.99 centile (149 h)	+4.7 °C	+4.5 °C	+3.8 °C	15%

3.3. Data Interpolation and Formatting

The data of each climate variable were first interpolated to the 1 h time-step, a typical standard for weather files for building simulations. The dry-bulb temperature, given in Kelvin was converted into Celsius (−273.15), the cloud cover, given in percentage, was converted into tenths; the specific humidity, given in kg/kg, was multiplied by thousands to convert to g/kg. Polynomial regressions were used for the dry-bulb temperature and the global solar radiation and linear regressions for the other weather variables. With the software EnergyPlus, different time–steps than one hour are possible; however, with the graphical interface DesignBuilder, only 1 h time–step weather files can be used. While using EnergyPlus, if a smaller time–step than 1 h is chosen, the internal EnergyPlus weather convertor linearly interpolates the weather variables to the smaller time–step. Six weather variables available every three hours were used, but others needed to be recalculated. Table 4 displays the data available from the NetCDF4 file and the data needed to reconstruct a weather file in the EPW format, typical for building simulations. We calculated the relative humidity and the dew-point temperature using the dry-bulb temperature, the specific humidity, and the atmospheric pressure (Equations (1)–(3)). We used the cloud cover used to calculate the direct normal radiation and the horizontal infrared radiation intensity (Equations (4)–(16)). The direct normal radiation could not be calculated using a standard solar model from the global horizontal radiation because values were given as an average every three hours, and were not a data point for this parameter, as well as for the cloud cover. We calculated the diffuse horizontal radiation from the global horizontal and the direct normal radiations. No future climate data exist on wind direction since it is not predictable in the long-term. Since the data is missing, we used the wind direction from an existing EPW file based on observations. Equations used to re-calculate the missing variables are detailed in this section.

In Equation (4), T the dry-bulb temperature (°C) was used to calculate VP_s, the saturated vapor pressure (hPa). In Equation (5) the water vapour pressure VP is calculated from AP, the atmospheric pressure (Pa), x the water content (g/kg), and $\varepsilon = 0.62198$. Both expressions are taken from the norm NF EN ISO 15927-1 [78]. From [79], the specific humidity is almost equal to the water content so the

water content was assumed equal to the specific humidity. Knowing the water vapour pressure VP and the saturated vapor pressure VP_s, the relative humidity RH (%) could be calculated (Equation (6)).

$$T > 0 : VP_s = 6.105 \times e^{\frac{17.269 \times T}{237.3+T}} \; T < 0 : VP_s = 6.105 \times e^{\frac{21.875 \times T}{265.5+T}} \quad (4)$$

$$VP = \frac{x \times \frac{AP}{100}}{\varepsilon + x} \quad (5)$$

$$RH = \frac{VP}{VP_s} \quad (6)$$

Table 4. Climate variable conversions from NetCDF4 files to EPW weather files for building thermal simulations. EURO-CORDEX = European Coordinated Regional Downscaling Experiment.

Climate Variable from EURO-CORDEX Every 3 h	Data Point Type	Interpolation Method to the Hourly Time-Step	Climate Variable Needed for the EPW File (Department of Energy, 2017)	Equations Used to Calculate the Missing Climate Variable
Dry-bulb temperature (K)	Data point *	Polynomial order $(n-1)$ with n the number of points per day	Dry-bulb Temperature (°C)	-
Specific Humidity (kg/kg)	Data point *	Linear	Relative Humidity (%), Dew-Point Temperature (°C)	Equations (1)–(3)
Atmospheric Pressure	Data point *	Linear	Atmospheric Pressure (Pa)	-
Cloud cover (%)	Average **	Linear	Direct Normal Radiation Horizontal Infrared Radiation Intensity (Wh/m^2)	Equations (4)–(14) and (17)–(18)
Global Horizontal Radiation (W/m^2)	Average **	Polynomial order $(n-1)$ with n the number of points per day	Diffuse Horizontal Radiation (Wh/m^2)	Equations (15)–(16)
Wind Speed (m/s)	Data point *	Linear	Wind Speed (m/s)	-
No climate variable	No data	-	Wind Direction (deg)	-

* Data point: Data available at 00 am, 03 am, 06 am, 09 am, 12 pm, 3 pm, 6 pm, 9 pm every day. ** Average: The data are averages from 0–3 am at the point 01.30 am, from 3–6 am at the point 04.30 am, etc., and at points 07.30 am, 10.30 am, 1.30 pm, 4.30 pm, 7.30 pm, and 10.30 pm every day.

Average data for the global horizontal radiation (GHR) were available every three hours. First, we set the GHR data points to zero when the sun was down, which was not systematically the case since data points are average (there could be a data point at 07.30 am, as an average from 06 am to 09 am, even if the sun was in reality down.) We then interpolated the data to the 30 min time-step and fit a polynomial through the existing data points, and the first and last zero data points each day (to recreate sunrise and sunset). Finally, we kept only the data points every hour to ensure consistency with the other climate data. We used the method introduced by [80] and then re-used by [51] to calculate the direct normal radiation while using the cloud cover data. The methodology used is described in the following.

We first discretised the extra-terrestrial spectral distribution of the solar radiation outside the atmosphere $i_0(\lambda)$ into 78 data points at 78 wavelengths (λ) from 115 nanometres (nm) to 5000 nm, so that each data point is an average of the spectral radiation between two consecutives λ. Then for each data point, we included the effects of the attenuation by the air mass and the turbidity, so $i_0(\lambda)$ became $i(\lambda)$ (Equation (7)).

$$i(\lambda) = i_0(\lambda).e^{-(\alpha_r + \alpha_d) \times m} \quad (7)$$

We then calculated, for each wave length, α_r the coefficient of absorption for molecular scatter (Equation (8)) and α_d the coefficient of absorption for particular scatter (Equation (9)) and m the optical air mass (Equation (10)) from Young [81]. In Equation (9), the turbidity coefficients β were taken from Taesler and Andersson [80]. In Equation (10), z_t the zenith angle in radians was calculated from

Equation (11) with h the sun height in degrees. The sun height was calculated using the Python PV-Lib module.

$$\alpha_{\mathrm{r}} = 0.00816 \times \lambda^{-4} \tag{8}$$

$$\alpha_{\mathrm{d}} = \beta \times \lambda^{-1.3} \tag{9}$$

$$m(z_{\mathrm{t}}) = \frac{1.002432 \times \cos^2(z_{\mathrm{t}}) + 0.148386 \times \cos(z_{\mathrm{t}}) + 0.0096467}{\cos^3(z_{\mathrm{t}}) + 0.149864 \times \cos^2(z_{\mathrm{t}}) + 0.0102963 \times \cos(z_{\mathrm{t}}) + 0.000303978} \tag{10}$$

$$z_{\mathrm{t}} = (h - 90) \times \frac{\pi}{180} \tag{11}$$

For each hour, we calculated the sum S of the attenuated radiation between two consecutive wavelengths (Equation (12)).

$$S = \sum_{\mathrm{n}=1}^{78} \left(\frac{i(\lambda)_{\mathrm{n}} + i(\lambda)_{\mathrm{n}+1}}{2} \right) \times \mathrm{e}^{-(\alpha_{\mathrm{r}} + \alpha_{\mathrm{d}}) \times m} \times (\lambda_{\mathrm{n}+1} - \lambda) \tag{12}$$

We added the effects of the cloud cover (CC) (Equation (13)).

$$S_1 = S \times (1 - CC) \tag{13}$$

We adjusted with the correction factor k, accounting for the variation during the year of the distance between the Earth and the sun (Equations (14) and (15)) with N_{d} the number of days per year and $w_{\mathrm{n}} = \frac{2\pi}{366}$

$$S_2 = k \times S_1 \tag{14}$$

$$\begin{aligned} k = \tfrac{1}{1353} \quad & \times (1353 + 45.326 \times \cos(w_{\mathrm{n}}) \times N_{\mathrm{d}} + 0.88018 \times \cos(2w_{\mathrm{n}}) \times N_{\mathrm{d}} \\ & -0.00461 \times \cos(3w_{\mathrm{n}}) \times N_{\mathrm{d}} + 1.8037 \times \sin(w_{\mathrm{n}}) \times N_{\mathrm{d}} + 0.097462 \\ & \times \sin(2w_{\mathrm{n}}) \times N_{\mathrm{d}} + 0.18412 \times \sin(3w_{\mathrm{n}}) \times N_{\mathrm{d}}) \end{aligned} \tag{15}$$

We calculated F, the water vapour present in the atmosphere (Equation (16)) from m (Equation (10)) and VP (Equation (5)) that we subtracted from S_2 in Equation (17) to finally calculate the direct normal radiation DNR.

$$F = 70 + 2.8 \times m \times VP \tag{16}$$

$$DNR = S_2 - F \tag{17}$$

We calculated the diffuse horizontal radiation DHR as the subtraction of the direct horizontal radiation $DN'R$ (Equation (18)) from the global horizontal radiation GHR (Equation (19)).

$$DN'R = DNR \times \sin(h) \tag{18}$$

$$DHR = GHR - DN\prime R \tag{19}$$

Finally, the horizontal infrared radiation intensity (LWR) was calculated by the EnergyPlus Weather Convertor (Equation (20)). The formula for the sky emissivity $\varepsilon_{\mathrm{sky}}$ is given in Equation (21), calculated from the cloud cover CC in tenths and the dew-point temperature and T_{dp}, calculated from the EnergyPlus Weather Convertor. TK is the dry-bulb temperature in Kelvin and σ is the Stefan-Boltzmann constant (5.6697×10^{-8}).

$$LWR = \varepsilon_{\mathrm{sky}} \times \sigma \times TK^4 \tag{20}$$

$$\varepsilon_{\mathrm{sky}} = \left(0.787 + 0.764 \times \ln\left(\frac{T_{\mathrm{dp}}}{273} \right) \right) \times \left(1 + 0.0244 \times CC - 0.0035 \times CC^2 + 0.00028 \times CC^3 \right) \tag{21}$$

3.4. Assembling Future Weather Files

3.4.1. Future Typical Year (TWY)

For building simulations, typical years are commonly used. A typical year is composed of 12 months issued from different years over a period of time (between 10 and 30 years). The selected months are the statistically most "typical" over the period. The selection process is explained in this section. Each country has its own method to reproduce typical years. The EPW format typical year format differs from the IWEC format or from the Typical Meteorological Year (TMY) format [27]. The main difference among the methods is the importance given to each climate parameter in the selection process. We used the methodology of the standard NF EN ISO 15927-4 [82] as it was used in France to reconstitute the typical year used for the French Thermal Regulation RT-2012. This method considers four climate parameters to select the most statistically common months among the years: The dry-bulb temperature, the relative humidity, the global horizontal radiation of equivalent first order, and the wind speed of second order. We created a Python code to automate the process to select the typical months. For selecting each month *mo*, the method is as follows: for each climate parameter p of first order, we sorted a series of daily averages in ascending order over the 30 year period, which allows to calculate the distribution function Φ (Equation (22)) over 30 years. Φ has 900 data points (N = 900) for months of 30 days. $L(i)$ is the rank in the series of the daily averages for the 30 years.

$$\Phi(p, mo, i) = \frac{L(i)}{N+1} \tag{22}$$

Secondly, we sort a series of daily averages also in ascending order for each year to calculate the distribution function ψ (Equation (23)) for each year y. $J(i)$ is the rank in the series of the daily averages for each year. ψ has 30 data points (n = 30) for a month of 30 days.

$$\psi(p, y, mo, i) = \frac{J(i)}{n+1} \tag{23}$$

The representation of the distribution functions Φ and ψ and the dry-bulb temperature classified in ascending order in January over the period 2041–2070 is presented on Table 5. We then compare the two distribution functions Φ and ψ for each year and for each month and calculate for each day i of the month n the difference $\psi - \Phi$ and then sum these absolute values for the considered month (Equation (24)), it is the Finkelstein-Schafer statistic (FS). We repeat this calculation for each month *mo* of each year y and for each climate parameter p of order 1.

$$FS(p, y, mo) = \sum_{i=1}^{n} \left| \psi(p, y, mo, i) - \Phi(p, mo, i) \right| \tag{24}$$

Table 5. Distribution functions Φ and ψ for one climate variable sorted in ascending order. Example for the dry-bulb temperature (p) over the period 2041–2070 in the month (*mo*) of January.

***L*(*i*)**	**Φ(*p*,*mo*,*i*)**	**Series of Daily Averages of the Climate Variable Classified in Ascending Order (Year 2041 to 2070)**	**ψ(*p*,*y*,*mo*,*i*)**	**Series of Daily Averages of the Climate Variable Classified in Ascending Order (*y* = 2041)**
1	0.0010	−7.75	0.03	−0.99
2	0.0021	−7.53	0.06	−0.48
3	0.0032	−7.52	0.09	−0.01

The final step allows to select the most typical months. We classified the *FS* in ascending order and for each month of each year for each climate parameter of first order, we attributed a rank. Then we summed the ranks of the three climate variables of first order (temperature, humidity, solar radiation)

and classified them by ascending order. For each month, the three lowest sums equivalent to three years are considered the three most typical years. The last climate variable, the wind speed, allows to determine which of these three pre-selected years is the most representative year. We sorted in ascending order the difference between the monthly average wind speed of each year with the monthly average wind speed of the 30 years. Finally, for each month, within the three pre-selected years, we selected the year with the lowest wind speed difference as being the typical year for this month. We repeated this process for each month, allowing to detect the twelve most typical months among the 30 years of data. We interpolated linearly for each climate variable of each month the eight last hours of the previous month and the next first eight hours of the following month.

We used this method to reassemble typical years for the three regional climate models HadGEM_RCA, IPSL_RCA and MPI_RCA over the historical (1976–2005) and future periods (2041–2070). To compare with the French weather file used by the Buildings Thermal Regulation (RT-2012) reconstructed with the same method from observations during the period 1994–2008, we also reassembled the typical years of these three models over the period 1991–2005 (closest period possible with the platform data availability for the historical multi-year projections). The hourly-extended summer (months from June to September) temperatures distribution of the three model typical years in Paris over the historical (1991–2005) and future (2041–2070) periods are shown on Figure 9.

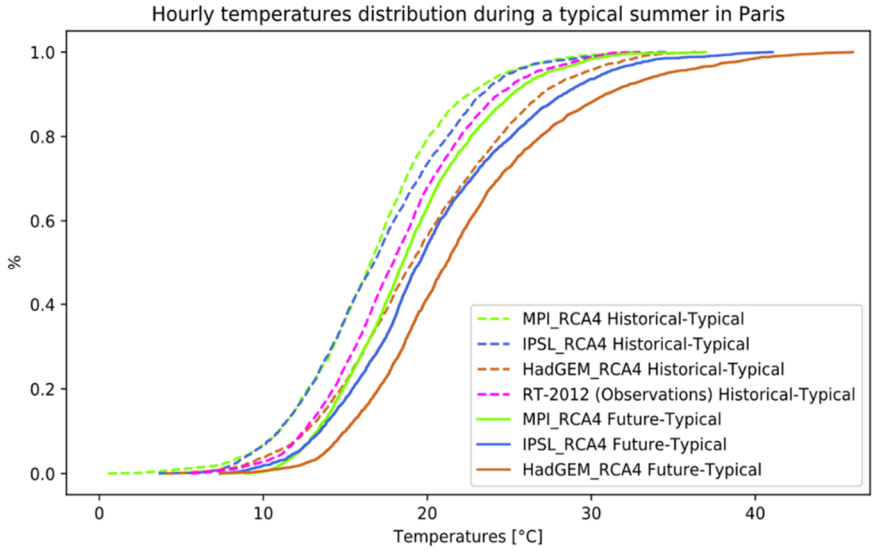

Figure 9. Hourly temperature distributions during a typical summer in Paris from three regional climate models (raw-outputs) and during the historical (1991–2005) and future (2041–2070) periods, scenario RCP 8.5.

During the historical period, the typical year summer hourly temperatures projected by the models MPI_RCA4 and IPSL_RCA4 over the historical period are lower than the observations (RT-2012) and the temperatures predicted by HadGEM_RCA4 are higher over the historical period 1994–2008. This can be explained by the fact that on Figure 9 we are analysing the raw-output data. These results are in line with the ones presented on Figure 8 since the bias-adjusted temperatures for the first two models are actually warmer and for HadGEM_RCA4 they are lower for the summer temperatures.

During the future period, the temperatures projected by the model MPI_RCA4 over the period 2041–2070 are really close to the data from RT-2012 (also expected from Figure 8). Since bias-adjusted future temperatures for the model IPSL_RCA are warmer than the raw outputs but colder for the model HadGEM_RCA, we can expect the future "real" summer temperatures to lay in between these two model projections (full blue and orange lines on Figure 9). Regarding the end of the distribution tail, the observed maximal temperatures during the historical typical year (RT-2012) were about 32 °C, they are projected to be around 40 °C during the future typical year.

3.4.2. Future Heatwave Event (HWE)

There is no consensus around the world over the definition of a heatwave. Numerous authors are studying the occurrence and intensity of future heatwaves and are using different indicators to identify them. Some authors detect heatwaves based on their impact on the population; others only consider the meteorological aspect, which is usually characterised as an extreme event on the temperature distribution over a reference period. In the United States, Robinson defined a heatwave based on daily minima and maxima temperature thresholds, calculated for each state based on body's reaction to temperature and humidity [83]. In Switzerland, Fischer and Schär detected a heatwave when the daily maximal temperature is above the 90th percentile of the temperature distribution over a reference period during at least five days. They characterise heatwaves by their amplitude (maximal temperature of the hottest yearly heatwave event), duration and frequency (number of heatwaves per year) [4]. In Australia, Nairn and Fawcett developed excess heat factor indices to detect heatwaves, based on three-days moving average of the daily mean temperature above the 95th percentile of the temperature distribution and on the previous 30 days daily mean temperature average to consider the population adaptation to the heatwave [84,85]. Perkins and Alexander defined two criteria, based on fifteen days moving average around the daily minimal and maximal temperatures [86]. Liu et al. have used percentiles correlated with mortality data after heatwaves in the UK [62]. Depending on the goal (building design, building resilience, population protection), heatwaves detection can be based on daily temperature maxima, minima or averages.

In France, a new method to detect heatwaves was recently adapted to a EURO-CORDEX dataset [67]. They used the basis of the operational method of heatwaves detection in France since 2006 that they updated to be suitable to any time series and to any spatial scale. The method was initially used for cold spells detections but has been adapted for heatwaves. The method is based on three percentile thresholds Spic, Sdeb, and Sint, which have been calculated based on mortality data due to historical heatwaves. They were originally absolute thresholds, and have been redefined as percentiles of the daily mean temperature distribution over several years in effort to make the method accessible to any dataset. Spic represents the threshold beyond which a heatwave event is detected (99.5 percentile of the temperature distribution over the historical period). Sdeb defines the beginning and the end of the heatwave (97.5 percentile) and Sint is the interruption threshold, used to merge two consecutive heatwave events without a significant drop in temperature (95 percentile). This method has been validated with the SAFRAN thermal indicator, previously used to detect French heatwaves by Ouzeau et al. in [26]. The method allows to characterise the heatwaves in term of maximal temperature, duration, and global intensity. A graphical representation of the heatwave detection is presented on Figure 10. We used this method to detect heatwaves in the 30 years temperatures series over the historical period 1976–2005 and the future period 2041–2070 (RCP 8.5) for the three selected climate models. On Figure 11, the famous bubble chart representation for heatwaves [67] is used to compare the heatwaves identified by the different climate models over the two periods. The 2003 heatwave (observations from the station Paris-Montsouris) is also shown in order to compare future and historical heatwaves with a well-known intense exceptional historical heatwave. The size of each bubble is characterised by its intensity. The intensity is the sum for each heatwave day of the positive difference between the daily mean temperature and the threshold Sdeb, divided by the difference between the Spic and Sdeb thresholds [87].

We detected heatwaves for both the raw-output and bias-adjusted temperatures for comparison. From Table 6, for the bias-adjusted data, we found the Spic, Sdeb, and Sint thresholds very similar; therefore, we used the thresholds median of the three models like in [67]. The thresholds are higher for the city of Paris than for the rest of France. For the raw-output, the thresholds differ greatly along the models (up to 3 °C difference) so we used each model threshold for heatwaves detection. Using thresholds specific to each dataset provided a consistent detection of the future heatwaves compared to the ones detected with the bias-adjusted temperatures (Figure 11). Since all the weather

variables are not available bias-adjusted, we use the raw-output data to build the future heatwave weather files.

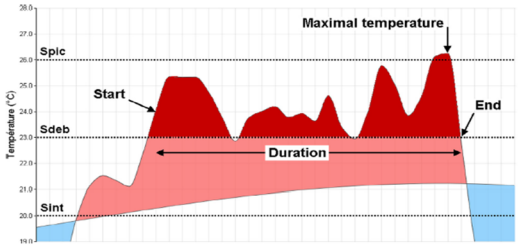

Figure 10. Heatwave detection from [67]. The Spic threshold is used for heatwave detection, the Sdeb threshold defines the heatwave duration, the Sint threshold ends the heatwave. Global intensity: read area of the plot in degree hours.

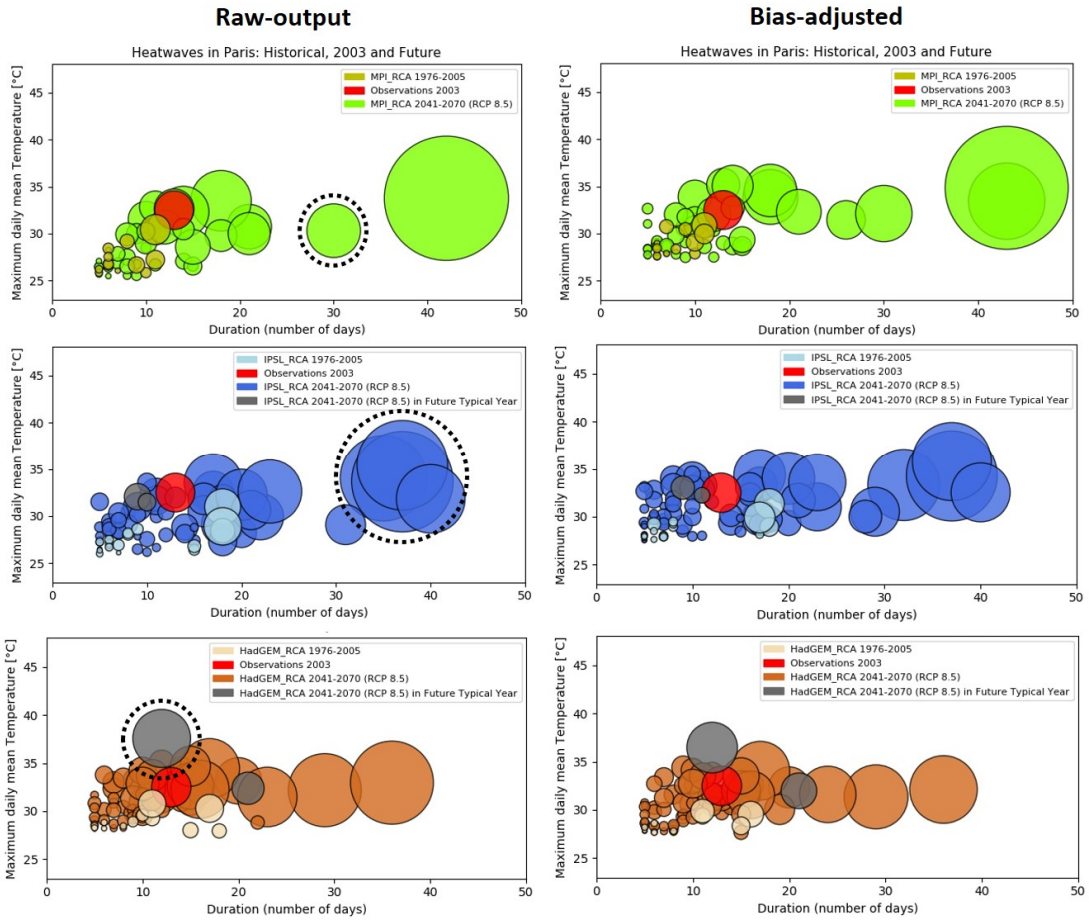

Figure 11. Heatwaves detected in Paris during the historical (1976–2005) and future (2041–2070 RCP 8.5) periods for the three RCMs for both raw-output and bias-adjusted temperatures. The 2003 heatwave (observations) is also displayed for comparison.

In comparison to historical heatwaves, future heatwaves are longer, more severe and with higher intensity. Depending on the model, they are times 3 to 4.5 more heatwaves in the future than the historical period. The models MPI_RCA, IPSL_RCA, and HadGEM projections are 42, 55, and 57 heatwaves during the future period, so at least and up to two per year in average. We found four future heatwaves more intense than the 2003 with the climate model MPI_RCA, seven with IPSL_RCA and six with HadGEM_RCA, suggesting one every 4.3 to 7.5 years between 2041 and 2070. We also found heatwaves in the future typical weather files reassembled from the model IPSL_RCA and

HadGEM_RCA, they are coloured in grey on Figure 11. Two heatwaves are found in the future typical year from IPSL_RCA, they are of lower intensity than in 2003. However, it is worth noticing that two consecutives heatwaves, one in July and one in August are found in the future typical year. In the future typical year from HadGEM_RCA, the heatwave found is the one with the highest maxima, and with a similar intensity than 2003. In fact, it occurs in the month of June of a particular warm year. This month was ranked fourth in temperature. Even though the month had very warm extreme temperatures, it also had colder temperatures, which allowed to rank it as typical. Once the other variables (humidity, solar radiation, and wind) were also considered, according to the standard ISO 15927-4, the month was ranked first and became a typical month. The difference in magnitude of the heatwaves found in the future typical years from the three climate models (zero HWE for MPI_RCA, two short HWE for IPSL_RCA, and one very high HWE for HadGEM_RCA) confirms the complementarity of the methodology in quantifying future HWE and not only re-assembling TWY.

Table 6. Thresholds for heatwave detection in Paris for three climate models.

Location	Data Type	Climate Model(s)	Sint (95)	Sdeb (97.5)	Spic (99.5)
Paris	Raw-output	MPI_RCA	20.76	22.27	25.40
Paris	Raw-output	IPSL_RCA	21.19	22.97	25.88
Paris	Raw-output	HadGEM_RCA	23.44	25.22	27.85
Paris	Raw-output	Median of the 3 models	21.19 (2.68)	22.97 (2.95)	25.88 (2.45)
Paris	Bias-adjusted	Median of the 3 models	22.9 (0.15)	24.39 (0.14)	27.48 (0.38)
France [67]	Bias-adjusted	Median of 11 models	20.67 (0.10)	22.03 (0.16)	24.27 (0.20)

We will analyse the building response to three different heatwaves, one from each model, highlighted in dotted-black on Figure 11. The heatwave from the MPI model is of similar intensity than the 2003 heatwave, but longer (one month) and with lower maxima. The heatwave from the IPSL model is a future "mega-heatwave" since it is very intense, long and with high maxima. The heatwave from the HadGEM model is the heatwave found in the future typical year: it is relatively short (twelve days), of similar intensity than in 2003 but with higher maxima.

After the 2003 heatwave in France, the Sanitary Watch Institute (INVS) established meteorological bio-indicators (IBM) to identify heatwaves and alert the population at the beginning of the heatwaves through a Heat Health Watch Warning System. The term bio indicates that the indicator is linked to a high mortality if it is above the thresholds, since the thresholds were calculated based on historical mortality data in pilot French cities. IBM is the couple (IBM_{min}, IBM_{max}) where IBM_{min} is the three-days moving daily minimal temperature and IBM_{max} the three-days moving daily maximal temperature. A heatwave is defined when the IBM couple (IBM_{min} and IBM_{max}) is above the thresholds during at least three days [88]. S_x and S_n are the thresholds for maximum and minimum temperatures, respectively; in Paris they are about 31 °C and 21 °C, and they are different for every French department. They are adjusted yearly to consider the population adaptation evolution to heat. In Figure 12, we show the IBM_{min} and IBM_{max} values for the three chosen heatwaves, and compared with the 2003 heatwave. We used the raw-output data as they are the only available to re-assemble the future weather files. The analysis could be improved by using the bias-adjusted data. However, during the selected HWE, the absolute temperature difference between the raw-output and bias-adjusted is relatively small as shown on Figure 11.

The HWE from the three models have IBM_{min} and IBM_{max} above their thresholds until day 14, except MPI_RCA under IBM_{min} from day 7. Moreover, for HadGEM_RCA and IPSL_RCA, the IBM_{min} and IBM_{max} are more intense than in 2003. A period when IBM_{min} is above S_n, combined to IBM_{max} above S_x usually relates to an intense prolonged heat period because the population cannot properly rest during the night because of the heat, which was the case in 2003. For these HWE, they are more intense than 2003 for around two weeks, but after the heat event is prolonged for two additional weeks even if the IBMs are lower. During the historical climate, no heatwave a month long was ever recorded in Paris neither in France; therefore, the effects of the building response on the occupants on such a

long period are not known. Indeed, the capacity of current naturally ventilated French buildings to protect the occupants from heat related health risk can be severely defeated by month-long heatwaves.

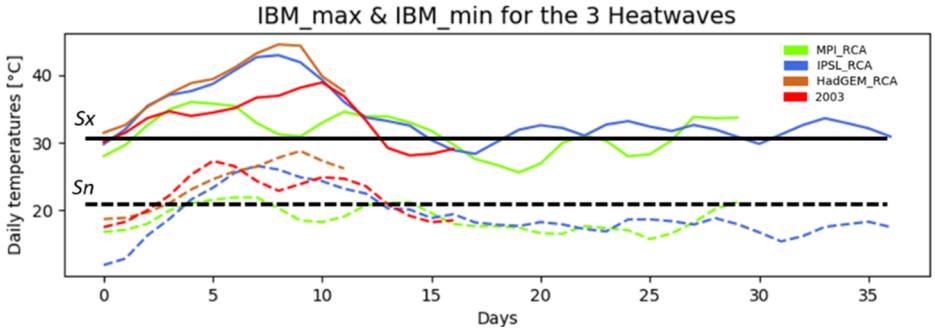

Figure 12. IBM_{min} and IBM_{max} values for the 3 future heatwaves in Paris compared to 2003.

Important parameters to characterise buildings overheating are the other climate parameters, mainly the direct solar radiation for the solar heat gains, the wind speed for the natural ventilation potential and the relative humidity for comfort. In Figure 13, these parameters are shown for the three future heatwaves. The heatwave modelled by MPI_RCA has a high direct radiation but a cloudy week (between days 17 and 24) during which it is also quite humid. The building indoors will have less solar heat gains but a higher humidity, which could increase discomfort. The heatwave from the model IPSL_RCA is sunny and with a moderate relative humidity. The HadGEM_RCA heatwave is sunny and dry with the humidity decreasing from the beginning until it reaches a minimal of 40% during the night and 20% during the day. All heatwaves exhibit wind speeds between 2 and 4 m/s.

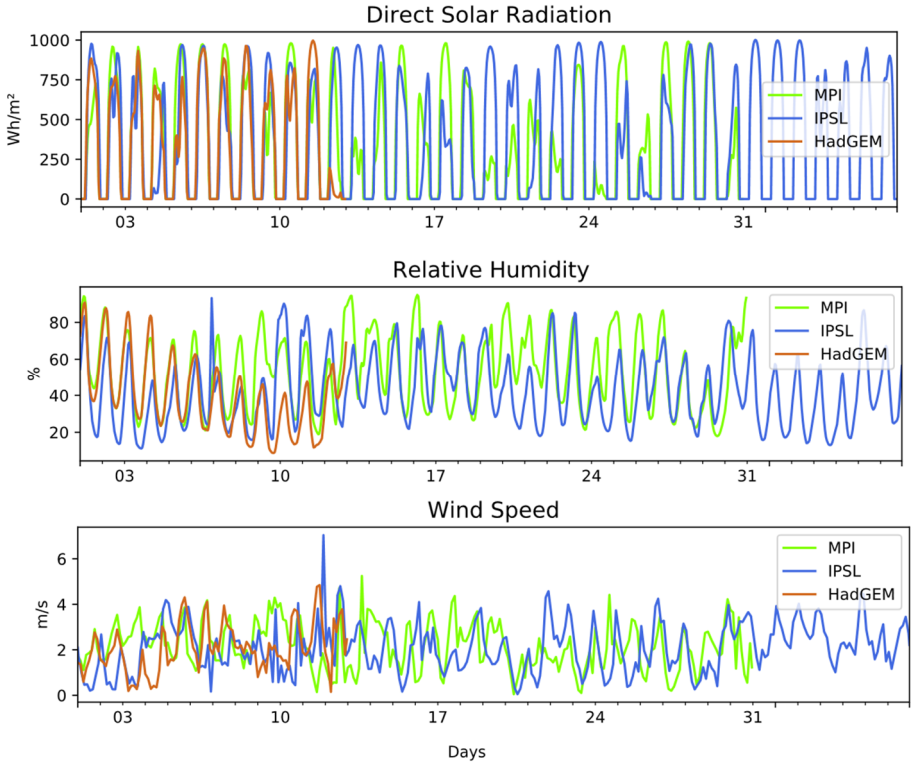

Figure 13. Direct normal solar radiation, relative humidity and wind speed for the three future heatwaves in Paris.

In this section, we presented two methods to build future weather files from the EURO-CORDEX future climate data. The TWY method is standard and already used by many building practitioners.

The HWE method is new and can be used for assessing building resilience to overheating under future heatwaves. As the method is percentile based, it allows to be used worldwide on any climate dataset. The French detection based on mortality thresholds is a supplementary indication of how often the heatwave alert would start according to the Heat Health Watch Warning System (HHWWS) included in the French National Heatwave Plan (NHP), if the adaptive capacities of organizations, populations and building infrastructure remained unchanged.

4. Using Future Weather Files for Building Simulations

In this section, we show an example of the use of TWY and HWE future weather files for building simulations for one building case study. We modelled a flat located on the top floor of a collective residential building with the graphic interface Design Builder v5.4 and the software EnergyPlus v8.6. The flat is composed of a 120 m^2 living space fully glazed on the North and South facades, with a 50 m^2 non-conditioned veranda oriented South and a 0.6 m width glazed cavity zone on the North façade, modelled as three distinct thermal zones (Figure 14).

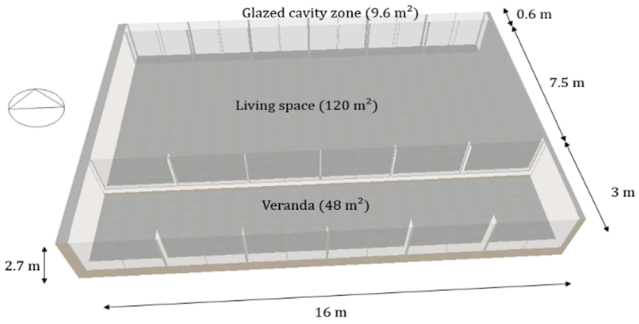

Figure 14. Representation of the apartment case study in Design Builder.

The verandas and glazed cavities allow reducing the winter heating needs, while act as buffer zones and enhance natural cross-ventilation during the summer. On each façade, one out of two windows can be opened. All windows operate with the same schedule: If the operative temperature in the zone reaches 20 °C, the windows are opened. We chose a low set point to enhance nocturnal natural ventilation. Windows are never opened when the exterior air is warmer than the interior. The ventilation is modelled with the Airflow Network of EnergyPlus. The South façade is equipped with light-coloured external shutters and a 1 m overhang. The shutters are used when the solar radiation on the incoming window is superior to 120 W/m^2. The exterior walls are made of 20 cm concrete with 14 cm external insulation, and the ceiling is made of 20 cm concrete with 15 cm insulation. The floor and the East wall were modelled adiabatic as they are in contact with adjacent apartments. All windows are double-glazing, except the exterior window of the veranda which is a single glazing. The apartment is occupied by five people with one person always present. The averaged heat produced by the individuals is 81 W, with a vesture of 0.3 clo during the summer. Future predictions of electric equipment in the next decades in France were used to calculate future internal gains, which correspond to 2.7 W/m^2 and 0.7 W/m^2 for the equipment and lights when the apartment is fully occupied [89].

The operative temperature of the living space during the historical and future TWY for the three RCMs is shown on Figure 15. For each model, we can quantify the temperature increase between the two TWY. For instance, at 50% of the hours from all the TWY, the temperature increase is of +0.8 °C, +1.2 and +1.5 for the models MPI_RCA, IPSL_RCA and HadGEM_RCA, respectively. At 95%, during hot summer temperatures of the typical years, the increase is of +1.8 °C, 3.2 °C and 3.5 °C, respectively. As for the exterior temperatures, the increase is superior for the hot temperatures. It is possible to conclude (considering model uncertainties) that the increase varies along these ranges.

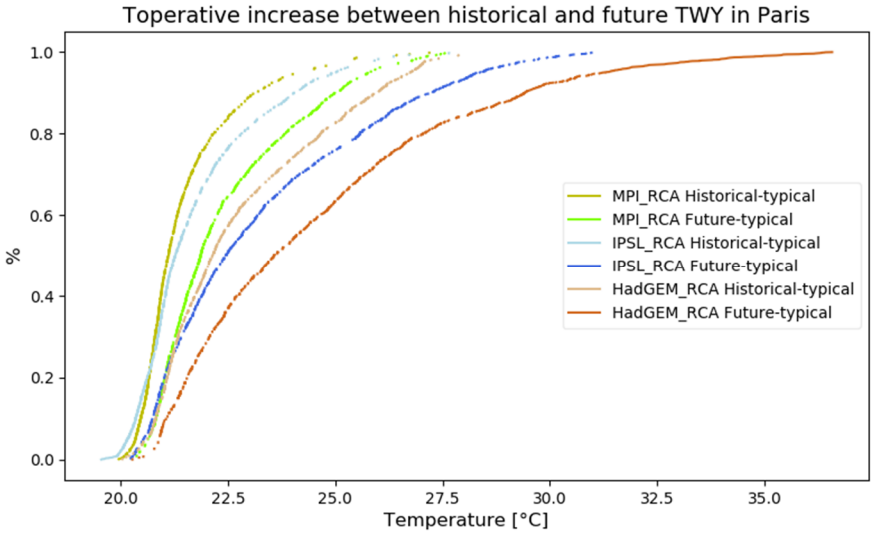

Figure 15. Summer operative temperature increase in the building case study between the historical (1976–2005) and future (2041–2070 RCP 8.5) TWY (typical years) in Paris from the three RCMs.

In Figure 16, the operative temperatures in the living space during the three heatwaves are displayed. The raw-output temperatures are used since the bias-adjusted ones are not available for all climate variables, from Figure 11 they were found to be relatively close even-though the bias-adjusted HWE temperatures are slightly lower. The HWE are highlighted in the colour of each model.

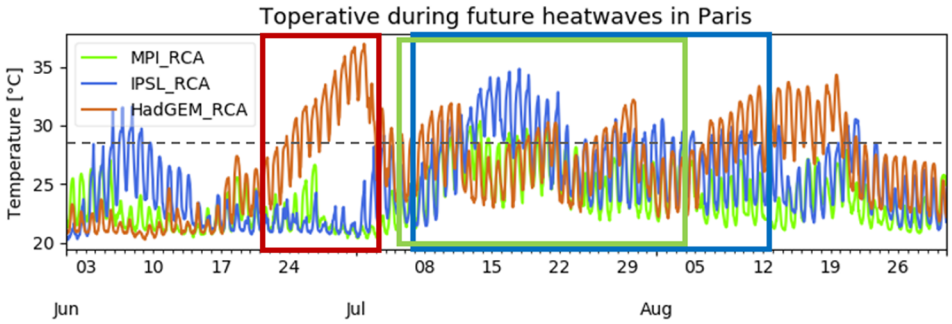

Figure 16. Summer operative temperatures in the building case study during the three future heatwaves in Paris.

During the heatwaves from the model IPSL_RCA and HadGEM_RCA, temperatures are often above the well-known simple threshold to assess building overheating at 28 °C. During the heatwave pics, even the night-time temperatures exceed 28 °C. The heatwave from HadGEM_RCA corresponds to the future typical month of June from that model, for which, even though typical, future operative temperatures during that month are very high. Temperatures decrease rapidly after the June HWE, however the summer of that HWE contains other heatwaves that hit successively the building, explaining the high temperatures later in August. During the long HWE from IPSL_RCA, it seems that after the most intense part of the heatwave (beginning of July), the building operative temperature return to acceptable levels even during the rest of the heatwave period. This can be explained by the fact that the bioclimatic building design greatly reduces the summer overheating thanks to the buffer spaces and an ideal use of the external shutters and of windows opening for night ventilation, even though we know that behavioural adaptations are not always optimized during overheating periods. Furthermore, vulnerable people have fewer possibilities to adapt, which results in increased building overheating; hence, thermal heat discomfort or heat stress is reached faster for these people most at risk. With a less favourable building design, operative temperatures could be much higher during future long HWE.

For the heatwave from the model MPI, temperatures rarely exceed 28 °C, which could be explained by the low solar gains during a period and lower external air temperatures compared to the other HWE. However, since the humidity is higher, the discomfort threshold will be lower. A comfort indicator including humidity should be used to analyse these indoor conditions. Even though we analysed some of the most intense heatwaves found over the future period 2041–2070, these would be "typical" heatwaves by the end of the century [67]. This analysis focused on indoor overheating but additional simulations were conducted to have an idea of the future heating and cooling energy needs and peak power. The living space of the flat was conditioned, with the external windows of the glazed cavity and of the veranda opened (to not overheat), and appropriate solar shading was used on the south glazed façade. For this building case study, the heating needs were divided by around two for all models when comparing the typical future and historical years. The cooling needs (really low during the historical year) were multiplied by a factor 3 to 4 for the future typical year depending on the climate model. The sum of heating and cooling needs was increased by a factor 1.2 to 1.5. The sizing of the heating systems could be reduced a little but not significantly, in contrast the cooling systems should be designed slightly larger. Surprisingly, the cooling demand did not peak extremely high during the future heatwaves (twice the sizing compared to the historical period); however, the cooling needs were 1.5 to 2.5 higher than the cooling needs for the future typical year (4 to 10 times higher than for the historical period).

5. Discussion

We proposed a methodology to reassemble future weather files for building simulations from EURO-CORDEX data. The method allows to detect future heatwaves from a multi-years dataset based on outdoor temperature thresholds and additional morbidity thresholds (IBMs). A very intense heatwave was found in the re-composed future typical year from one climate model, which might question the weighting of weather variables in the reconstruction method for future typical years, especially for free-running buildings sensitive to external temperature. Nik has proposed a method to reconstruct both future typical years and future extreme years, using only the dry-bulb temperature to select the months [59]. Using a similar approach would even out the probability to discover a very intense heatwave in the future typical year; however, the future typical year could have particularly low solar radiation, high wind speed or particularly high or low humidity, three important weather parameters that might underestimate future overheating risks or cooling loads in buildings. Our method is flexible and allows to choose heatwaves based on the analysis of other weather variables as well.

Most authors who re-assembled or used future typical years have used them to quantify the future building energy demand [59,90]. In that case, statistical downscaled climate data such as the one derived from the morphing methods can easily be used for such assessments. Authors have used future typical or future extreme years to estimate the peak load of air-conditioning systems [50,91,92]. In contrast, authors who analysed the future thermal indoor environment of buildings usually did not use future typical or extreme years, but either historical observations of heatwaves in order to recreate indoor hot conditions [93]. Our method is new since it allows to analyse buildings indoor conditions with future heatwaves.

Only a few researchers have correlated warm indoor temperatures during heatwaves and buildings resilience to heat related morbidity risk, most research being about outdoor temperatures. Liu et al. used the UKCP09 weather generator to generate 3000 future probabilistic weather files and selected the ones containing heatwaves based on three different threshold criteria for England to conduct building thermal simulations. They finally could define future "deadly" heatwaves based on morbidity assessment of future indoor temperatures using morbidity thresholds from historical observations and considering peoples adaptation to heat. They also calculated that the indoor threshold for building resilience against deadly heatwaves could be increased as much as +4 °C by 2080, considering both building and occupant adaptations [62]. We could use a similar approach for further study, using the

IBM thresholds, built from historical morbidity data in France, to select the heatwaves that would have a strong impact on the indoor environment. This could already be observed from Figures 12 and 16, since only the two heatwaves from the models HadGEM_RCA and IPSL_RCA were above both the IBM_{max} and IBM_{min} thresholds, and resulted in stronger indoor operative temperatures than for the heatwave MPI_RCA, which was below the IBM_{min} threshold. An indicator to detect heatwaves on minimal daily temperatures (IBM_{min} thresholds) is often not used by researchers even though it is well known that elevated night-temperatures have a strong impact on morbidity during heatwaves since people might be prevented from sleep and rest. A relative threshold of 95% percentile of the minimum temperature was used by [94] to find hot night hours and to calculate a hot night degree index, leading to an estimation of the intensity of nocturnal thermal stress. Guo et al. used a daily minimal temperature absolute threshold of 26.7 °C, using the same one as Robinson [83,95]. The heatwaves detection method we used is based on relative thresholds, which allows the replicability of the method in another climate. Furthermore, to evaluate people's ability to withstand elevated indoor thermal stress, appropriate discomfort or heat stress indicators need to be used; this will be the work of future research. An indicator considering not only the dry-bulb temperature, but also humidity conditions, solar radiation, and wind speed should be used, such as the Wet-bulb Globe Temperature (WBGT). However, this indicator has limitations, since it was used for healthy military workers, and in the case of building morbidity, people the most at risk are vulnerable, so the thresholds will most likely be lower.

Because of the difficulty to find future climate data, only a few authors have used several RCMs for building simulation. As a result of the recently available CORDEX data, multi-ensemble assessments will probably become a common practice in the building community. Climate uncertainties (in both the RCP scenario and the climate model) can be used to help stakeholders to assess risk. Coley et al. compared changes in internal temperatures for three future probabilistic years (10%, 50%, and 90%) and observed that depending on the selected future climate the scale of the adaptations needed would be very different. They pointed out that the risk assessment is left to building designers and that the design approach will be conditioned by the designer's approach to risk. Furthermore, they suggest one approach: Using median future projections for designing buildings, leaving opportunity to behavioural adaptation under warmer than expected temperatures [96].

The indicator used to detect heatwaves in this paper was made in the context of the Extremoscope project, which was mandated by the French ministry of ecology as part of their national adaptation plan and for urban heat island monitoring. Future heatwaves have been used to evaluate the cities resilience to climate change [97], but little work has been done to evaluate the buildings resilience to future heatwaves, this work wishes to be a stepping-stone. In France, future TWY and HWE could be used at national level for risk assessment of buildings resilience to climate change and their capacity to protect the occupants under future heatwaves.

Limitations of this work include the fact that for the moment, as bias-adjusted data are not available for all weather variables necessary to reconstruct future weather files ready-to-use for building simulations, only comparative impact assessments can be done. This is the current practice of the building community, and it is sufficient to provide guidelines for buildings adaptation to climate change. However, it might be limited for the design or risk analyses, which require absolute thresholds. Furthermore, urban effects are not included in these weather files; it is a topic that will be investigated further. Future research directions include the use of these weather files for building risk assessment under future heatwaves, and the choice of appropriate indicators to assess the building resilience. Additionally, these weather files have been made to assist in the design stage of the building to guide building practitioners in the implementation of passive cooling strategies in cases where air-conditioning can be limited. The investigation of various strategies for building adaptation and mitigation to climate change is currently under research [98]. Other areas of work would be to optimise the building design, not only in terms of thermal comfort and energy consumption [99,100], but also considering life-cycle analysis of building materials, cost of the various strategies, and policy

incentives [101,102]. Finally, these future weather files can also be used to help in the design of renewable energy systems under future typical and extreme conditions, similarly to [103].

6. Conclusions

In this paper, we first described the different methods that are used by the building community to re-assemble or re-create future climate data. The literature review highlighted a need to produce future weather files containing hot temperature extremes, such as heatwaves. We proposed a methodology for assembling ready-to-use future weather files for building simulations. We presented both future typical weather year (TWY) and heatwave event (HWE) weather files, allowing to assess the building's indoor conditions under future typical conditions and future heatwaves. We used the climate multi-year projections from the EURO-CORDEX project, very recently available on a 12.5 km spatial resolution. For the first time, a methodology was presented to use these climate data for building simulations. The methodology allowed to interpolate the climate data from datasets every three hours to every hour and calculate missing data to reconstitute future ready-to-use weather files. We reassembled historical and future typical weather files (TWY) and future heatwave events (HWE) based on a climate criterion and additional morbidity data, and differentiated them, not only in terms of dry-bulb temperature, but also relative humidity, direct solar radiation, and wind speed. We modelled a building case-study located in Paris with the software EnergyPlus and used these new future weather files to analyse potential building overheating and building resilience to future heatwaves by comparing future to historical climate projections. Finally, we considered the uncertainties related to the climate models by using three models (one RCM downscaled from three GCMs) to calculate the building's indoor conditions. Because of the method chosen to reconstruct future typical weather files, future HWE may or may not already be included in future TWY. This highlighted the need of the additional method proposed to detect future HWE. As of today, the use of these future climate data is limited to relative comparisons, since bias-adjusted data are not available for all climate variables needed to reassemble future weather files for building simulations. This is the current practice in building simulations with future weather files, and if data were bias-adjusted, an analysis in relative values would be more straightforward. Various bias-adjustment methods exist and it is also possible to use one. However, if raw-output temperatures are close to the bias-adjusted ones, such as for the selected HWE, even the raw-output data allow an analysis in absolute values. The analysis with the future HWE enhanced the need to assess future indoor extreme conditions, or serious overheating and heat stress could occur if appropriate adaptation strategies were not taken. Heatwaves will only increase in duration, intensity, and severity towards the end of the century, which coincide with the lifetime of a building built today. This proposed methodology is addressed to both researchers and building practitioners who are looking for future weather files to analyse the required adaptations of building and energy systems to climate change towards the end of the century.

Author Contributions: Conceptualization, methodology, formal analysis C.I., J.-M.A., C.P., J.R., and A.M.; investigation, validation, data curation, writing—original draft preparation A.M.; Writing—review and editing, A.M., C.I., J.-M.A.; Supervision, C.I., J.-M.A., C.P., J.R.; Funding acquisition, C.I., C.P. All authors have read and agreed to the published version of the manuscript.

Funding: This research was partially funded by La Région Aquitaine.

Acknowledgments: The authors would like to thank Jean-Louis Dufresne for his communication, knowledge, and help to use the CORDEX projections. The authors acknowledge the World Climate Research Programme's Working Group on Regional Climate, and the Working Group on Coupled Modelling, former coordinating body of CORDEX and responsible panel for CMIP5. The authors thank the climate modelling groups (listed in Table 2 of this paper) for producing and making available their model output. The authors acknowledge the Earth System Grid Federation infrastructure an international effort led by the U.S. Department of Energy's Program for Climate Model Diagnosis and Intercomparison, the European Network for Earth System Modelling and other partners in the Global Organisation for Earth System Science Portals (GO-ESSP). The authors thank Antoine Falaize and Fanny Devys-Peyre for their help with programming the Python code to compile the future weather files. The authors finally thank the anonymous reviewers whose comments helped to improve this manuscript.

Data and Code Availability: The Python code to reproduce the future weather files for building simulations is available from the corresponding author for academic purposes upon request. The raw climate data are available from EURO-CORDEX (https://www.cordex.com).

Conflicts of Interest: The authors declare no conflict of interest.

References

1. Kjellström, E.; Nikulin, G.; Strandberg, G.; Bøssing Christensen, O.; Jacob, D.; Keuler, K.; Lenderink, G.; Van Meijgaard, E.; Schär, C.; Somot, S.; et al. European climate change at global mean temperature increases of 1.5 and 2 °C above pre-industrial conditions as simulated by the EURO-CORDEX regional climate models. *Earth Syst. Dyn.* **2018**, *9*, 459–478. [CrossRef]
2. Meehl, G.A.; Tebaldi, C. More intense, more frequent, and longer lasting heat waves in the 21st century. *Science* **2004**, *305*, 994–997. [CrossRef] [PubMed]
3. Beniston, M.; Stephenson, D.B.; Christensen, O.B.; Ferro, C.A.T.; Frei, C.; Goyette, S.; Halsnaes, K.; Holt, T.; Jylhä, K.; Koffi, B.; et al. Future extreme events in European climate: An exploration of regional climate model projections. *Clim. Chang.* **2007**, *81*, 71–95. [CrossRef]
4. Fischer, E.M.; Schär, C. Consistent geographical patterns of changes in high-impact European heatwaves. *Nat. Geosci.* **2010**, *3*, 398–403. [CrossRef]
5. Bador, M.; Terray, L.; Boé, J.; Somot, S.; Alias, A.; Gibelin, A.L.; Dubuisson, B. Future summer mega-heatwave and record-breaking temperatures in a warmer France climate. *Environ. Res. Lett.* **2017**, *12*, 074025. [CrossRef]
6. Bessemoulin, P.; Bourdette, N.; Courtier, P.; Manach, J. La canicule d'août 2003 en France et en Europe. *La Météorologie* **2004**, *8*, 25. [CrossRef]
7. Rousseau, D. *La Météorologie*; Société Météorologique de France: Paris, France, 2005. [CrossRef]
8. Hémon, D.; Jougla, E. La canicule du mois d'août 2003 en France. *Rev. Epidemiol. Sante Publique* **2004**, *52*, 3–5. [CrossRef]
9. Grignon-Massé, L.; Rivière, P.; Adnot, J. Strategies for reducing the environmental impacts of room air conditioners in Europe. *Energy Policy* **2011**, *39*, 2152–2164. [CrossRef]
10. Santamouris, M. Cooling the buildings—Past, present and future. *Energy Build.* **2016**, *128*, 617–638. [CrossRef]
11. International Energy Agency. *The Future of Cooling Opportunities for Energy—Efficient Air Conditioning*; International Energy Agency: Paris, Franch, 2018.
12. Steffen, W.; Hughes, L.; Perkins, S. *Heatwaves: Hotter, Longer, More Often*; Climate Council of Australia: Potts Point, Australia, 2014; ISBN 9780992414221.
13. Reeves, J.; Foelz, C.; Grace, P.; Best, P.; Marcussen, T.; Mushtaq, S.; Stone, R.; Loughnan, M.; McEvoy, D.; Ahmed, I.; et al. *Impacts and Adaptation Responses of Infrastructure and Communities to Heatwaves: The Southern Australian Experience of 2009*; National Climate Change Adaptation Research Facility: Southport, Austrilia, 2010.
14. Ke, X.; Wu, D.; Rice, J.; Kintner-Meyer, M.; Lu, N. Quantifying impacts of heat waves on power grid operation. *Appl. Energy* **2016**, *183*, 504–512. [CrossRef]
15. Totschnig, G.; Hirner, R.; Müller, A.; Kranzl, L.; Hummel, M.; Nachtnebel, H.P.; Stanzel, P.; Schicker, I.; Formayer, H. Climate change impact and resilience in the electricity sector: The example of Austria and Germany. *Energy Policy* **2017**, *103*, 238–248. [CrossRef]
16. Ribéron, J.; Vandentorren, S.; Bretin, P.; Zeghnoun, A.; Salines, G.; Cochet, C.; Thibault, C.; Hénin, M.; Ledrans, M. Building and Urban Factors in Heat Related Deaths during the 2003 Heat Wave in France. In Proceedings of the Healthy Buildings Conference, Lisboa, Portugal, 4–8 June 2006.
17. Vandentorren, S.; Bretin, P.; Zeghnoun, A.; Mandereau-Bruno, L.; Croisier, A.; Cochet, C.; Ribéron, J.; Siberan, I.; Declercq, B.; Ledrans, M. August 2003 heat wave in France: Risk factors for death of elderly people living at home. *Eur. J. Public Health* **2006**, *16*, 583–591. [CrossRef] [PubMed]
18. Liu, C.; Kershaw, T.; Fosas, D.; Ramallo Gonzalez, A.P.; Natarajan, S.; Coley, D.A. High resolution mapping of overheating and mortality risk. *Build. Environ.* **2017**, *122*, 1–14. [CrossRef]
19. Taylor, J.; Wilkinson, P.; Picetti, R.; Symonds, P.; Heaviside, C.; Macintyre, H.L.; Davies, M.; Mavrogianni, A.; Hutchinson, E. Comparison of built environment adaptations to heat exposure and mortality during hot weather, West Midlands region, UK. *Environ. Int.* **2018**, *111*, 287–294. [CrossRef]

20. ASHRAE. Chapter 14, Climatic Design Information. In *ASHRAE Handbook—Fundamentals 2017*; ASHRAE: Peachtree Corners, GA, USA, 2017.
21. Hacker, J.N.; Belcher, S.E.; Andrew, W. *Design Summer Years for London CIBSE TM49: 2014*; CIBSE: London, UK, 2014.
22. Ministère de la Transition Ecologique et Solidaire RE2020: Une Nouvelle Etape vers une Future Règlementation Environnementale des Bâtiments Neufs plus Ambitieuse Contre le Changement Climatique. Available online: https://www.ecologique-solidaire.gouv.fr/re2020-nouvelle-etape-vers-future-reglementation-environnementale-des-batiments-neufs-plus (accessed on 16 April 2020).
23. Miller, W.; Machard, A.; Bozonnet, E.; Yoon, N.; Qi, D.; Zhang, C.; Liu, A.; Sengupta, A.; Akander, J.; Hayati, A.; et al. How can we define and measure "resilient cooling"?—A review and evaluation of resilience frameworks and criteria. *Submitt. Appl. Energy* **2020**. submitted for publication.
24. Folland, C.K.; Karl, T.R.; Christy, J.R.; Clarke, R.A.; Gruza, G.V.; Jouzel, J.; Mann, M.E.; Oerlemans, J.; Salinger, M.J.; Wang, S.-W. 2001: Observed Climate Variability and Change. In *Climate Change 2001: The Scientific Basis*; Contribution of Working Group I to the Third Assessment Report of the Intergovernmental Panel on Climate Change; Hougton, J.T.Y., Ding, D.J., Griggs, M., Noguer, P., Eds.; Cambridge University Press: Cambridge, UK, 2001; p. 881.
25. Giorgi, F. Climate change prediction. *Clim. Chang.* **2005**, *73*, 239–265. [CrossRef]
26. Ouzeau, G.; Déqué, M.; Jouini, M.; Planton, S.; Vautard, R.; Jouzel, J. *Le Climat de la France au XXIème siècle Volume 4. Scénarios régionalisés: Édition 2014 pour la métropole et les régions d'outre-mer*; Rapports de la Direction générale de l'Énergie et du Climat: Paris, France, 2014.
27. Herrera, M.; Natarajan, S.; Coley, D.A.; Kershaw, T.; Ramallo-González, A.P.; Eames, M.; Fosas, D.; Wood, M. A review of current and future weather data for building simulation. *Build. Serv. Eng. Res. Technol.* **2017**, *38*, 602–627. [CrossRef]
28. Hawkins, E.; Sutton, R. The potential to narrow uncertainty in regional climate predictions. *Bull. Am. Meteorol. Soc.* **2009**, *90*, 1095–1108. [CrossRef]
29. Hawkins, E.; Sutton, R. The potential to narrow uncertainty in projections of regional precipitation change. *Clim. Dyn.* **2011**, *37*, 407–418. [CrossRef]
30. Belcher, S.; Hacker, J.; Powell, D. Constructing design weather data for future climates. *Build. Serv. Eng. Res. Technol.* **2005**, *26*, 49–61. [CrossRef]
31. Jentsch, M.F.; James, P.A.B.; Bourikas, L.; Bahaj, A.B.S. Transforming existing weather data for worldwide locations to enable energy and building performance simulation under future climates. *Renew. Energy* **2013**, *55*, 514–524. [CrossRef]
32. Jentsch, M.F.; Bahaj, A.B.S.; James, P.A.B. Climate change future proofing of buildings-Generation and assessment of building simulation weather files. *Energy Build.* **2008**, *40*, 2148–2168. [CrossRef]
33. Jentsch, M.F. Technical Reference Manual for the CCWeatherGen and CCWorldWeatherGen tools Version 1.2. 2012. Available online: energy.soton.ac.uk/files/2013/06/technical_reference.pdf (accessed on 31 October 2017).
34. Troup, L.; Fannon, D. Morphing Climate Data to Simulate Building Energy Consumption. In Proceedings of the ASHRAE and IBPSA-USA SimBuild 2016 Building Performance Modeling Conference, Salt Lake City, UT, USA, 10–12 August 2016; pp. 439–446.
35. Moazami, A.; Carlucci, S.; Geving, S. Critical Analysis of Software Tools Aimed at Generating Future Weather Files with a view to their use in Building Performance Simulation. *Proc. Energy Procedia* **2017**, *132*, 640–645. [CrossRef]
36. Troup, L.; Eckelman, M.J.; Fannon, D. Simulating future energy consumption in office buildings using an ensemble of morphed climate data. *Appl. Energy* **2019**, *255*, 113821. [CrossRef]
37. Meteonorm. Handbook Part II: Theory, Version 7.2. Global Meteorological Database Version 7, Software and Data for Engineers, Planers and Education. The Meteorological Reference for Solar Energy Applications, Building Design, Heating & Cooling Systems, Education Rene. 2017. Available online: https://meteonorm.com/assets/downloads/mn73_software.pdf (accessed on 1 February 2018).
38. Jones, P.; Harpham, C.; Kilsby, C.; Glenis, V.; Burton, A. UK Climate Projections Science Report: Projections of Future Daily Climate for the UK from the Weather Generator. 2010. Available online: https://eprint.ncl.ac.uk/file_store/production/217986/B1B47084-F4B6-446C-A750-8E47554D8B7F.pdf (accessed on 3 November 2019).
39. Kershaw, T.; Eames, M.; Coley, D. Assessing the risk of climate change for buildings: A comparison between multi-year and probabilistic reference year simulations. *Build. Environ.* **2011**, *46*, 1303–1308. [CrossRef]

40. Wang, L.; Mathew, P.; Pang, X. Uncertainties in energy consumption introduced by building operations and weather for a medium-size office building. *Energy Build.* **2012**, *53*, 152–158. [CrossRef]
41. Zhai, Z.J.; Helman, J.M. Climate change: Projections and implications to building energy use. *Build. Simul.* **2019**, *12*, 585–596. [CrossRef]
42. Lhotka, O.; Kyseley, J.; Plavcova, E. Evaluation of major heat waves' mechanisms in EURO-CORDEX RCMs over Central Europe. *Clim. Dyn.* **2017**, *50*, 4249–4262. [CrossRef]
43. Koffi, B.; Koffi, E. Heat waves across Europe by the end of the 21st century: Multiregional climate simulations. *Clim. Res.* **2008**, *36*, 153–168. [CrossRef]
44. Vautard, R.; Gobiet, A.; Jacob, D.; Belda, M.; Colette, A.; Déqué, M.; Fernández, J.; García-Díez, M.; Goergen, K.; Güttler, I.; et al. The simulation of European heat waves from an ensemble of regional climate models within the EURO-CORDEX project. *Clim. Dyn.* **2013**, *41*, 2555–2575. [CrossRef]
45. Giorgi, F. Thirty Years of Regional Climate Modeling: Where Are We and Where Are We Going next? *J. Geophys. Res. Atmos.* **2019**, *124*, 5696–5723. [CrossRef]
46. Jacob, D.; Petersen, J.; Eggert, B.; Alias, A.; Christensen, O.B.; Bouwer, L.M.; Braun, A.; Colette, A.; Déqué, M.; Georgievski, G.; et al. EURO-CORDEX: New high-resolution climate change projections for European impact research. *Reg. Environ. Chang.* **2014**, *14*, 563–578. [CrossRef]
47. Kotlarski, S.; Keuler, K.; Christensen, O.B.; Colette, A.; Déqué, M.; Gobiet, A.; Goergen, K.; Jacob, D.; Lüthi, D.; Van Meijgaard, E.; et al. Regional climate modeling on European scales: A joint standard evaluation of the EURO-CORDEX RCM ensemble. *Geosci. Model. Dev.* **2014**, *7*, 1297–1333. [CrossRef]
48. WRCP Coordinated Downscaling Experiment—European Domain. Available online: https://www.euro-cordex.net/ (accessed on 27 November 2019).
49. EUROCORDEX Cordex Archive Specifications. Available online: https://is-enes-data.github.io/cordex_archive_specifications.pdf (accessed on 1 April 2018).
50. Moazami, A.; Nik, V.M.; Carlucci, S.; Geving, S. Impacts of future weather data typology on building energy performance—Investigating long-term patterns of climate change and extreme weather conditions. *Appl. Energy* **2019**, *238*, 696–720. [CrossRef]
51. Nik, V.M. *Climate Simulation of an Attic Using Future Weather Data Sets—Statistical Methods for Data Processing and Analysis*; Chalmers University Of Technology: Göteborg, Sweden, 2010.
52. Giorgi, F. Regional climate modeling: Status and perspectives. *J. Phys. IV EDP Sci.* **2006**, *139*, 101–118. [CrossRef]
53. Mearns, L.O.; Giorgi, F.; Whetton, P.; Pabon, D.; Hulme, M.; Lal, M. *Guidelines for Use of Climate Scenarios Developed from Regional Climate Model Experiments*; IPCC: Geneva, Switzerland, 2003.
54. Lewis, S.C.; King, A.D. Evolution of mean, variance and extremes in 21st century temperatures. *Weather Clim. Extrem.* **2017**, *15*, 1–10. [CrossRef]
55. Russo, S.; Dosio, A.; Graversen, R.G.; Sillmann, J.; Carrao, H.; Dunbar, M.B.; Singleton, A.; Montagna, P.; Barbola, P.; Vogt, J.V. Magnitude of extreme heat waves in present climate and their projection in a warming world. *J. Geophys. Res. Atmos.* **2014**, *119*, 12500–12512. [CrossRef]
56. Alessandrini, J.M.; Ribéron, J.; Da Silva, D. Will naturally ventilated dwellings remain safe during heatwaves? *Energy Build.* **2019**, *183*, 408–417. [CrossRef]
57. Synnefa, A.; Garshasbi, S.; Haddad, S.; Paolini, R.; Santamouris, M. Impact of the mitigation of the local climate on building energy needs in Australian cities. In Proceedings of the Engaging Architectural Science: Meeting the Challenges of Higher Density: 52nd International Conference of the Architectural Science Association 2018, Melbourne, Australia, 28 November–1 December 2018; pp. 277–284.
58. Pyrgou, A.; Castaldo, V.L.; Pisello, A.L.; Cotana, F.; Santamouris, M. On the effect of summer heatwaves and urban overheating on building thermal-energy performance in central Italy. *Sustain. Cities Soc.* **2017**, *28*, 187–200. [CrossRef]
59. Nik, V.M. Making energy simulation easier for future climate—Synthesizing typical and extreme weather data sets out of regional climate models (RCMs). *Appl. Energy* **2016**, *177*, 204–226. [CrossRef]
60. Ramon, D.; Allacker, K.; van Lipzig, N.P.M.; De Troyer, F.; Wouters, H. Future Weather Data for Dynamic Building Energy Simulations: Overview of Available Data and Presentation of Newly Derived Data for Belgium. In *Energy Sustainability in Built and Urban Environments*; Springer: Berlin/Heidelberg, Germany, 2018; pp. 111–138.

61. Liu, C.; Kershaw, T.; Eames, M.E.; Coley, D.A. Future probabilistic hot summer years for overheating risk assessments. *Build. Environ.* **2016**, *105*, 56–68. [CrossRef]
62. Liu, C.; Chung, W.-J.; Coley, D. Creation Of Future Hot Event Years For Assessing Building Resilience Against Future Deadly Heatwaves. In Proceedings of the IBPSA 2019—International Building Performance Simulation Association 2019, Rome, Italy, 2–4 September 2019; Liu, C., Chung, W.-J., Coley, D., Eds.; Centre for Energy and the Design of Environments, University of Bath: Bath, UK, 2019.
63. Jentsch, M.F.; Eames, M.E.; Levermore, G.J. Generating near-extreme Summer Reference Years for building performance simulation. *Build. Serv. Eng. Res. Technol.* **2015**, *36*, 701–721. [CrossRef]
64. Du, H.; Underwood, C.P.; Edge, J.S. Generating design reference years from the UKCP09 projections and their application to future air-conditioning loads. *Build. Serv. Eng. Res. Technol.* **2012**, *33*, 63–79. [CrossRef]
65. Lemonsu, A.; Beaulant, A.L.; Somot, S.; Masson, V. Evolution of heat wave occurrence over the Paris basin (France) in the 21st century. *Clim. Res.* **2014**, *61*, 75–91. [CrossRef]
66. Lemonsu, A.; Viguié, V.; Daniel, M.; Masson, V. Vulnerability to heat waves: Impact of urban expansion scenarios on urban heat island and heat stress in Paris (France). *Urban. Clim.* **2015**, *14*, 586–605. [CrossRef]
67. Ouzeau, G.; Soubeyroux, J.M.; Schneider, M.; Vautard, R.; Planton, S. Heat waves analysis over France in present and future climate: Application of a new method on the EURO-CORDEX ensemble. *Clim. Serv.* **2016**, *4*, 1–12. [CrossRef]
68. Nik, V.M.; Sasic Kalagasidis, A.; Kjellström, E. Statistical methods for assessing and analysing the building performance in respect to the future climate. *Build. Environ.* **2012**, *53*, 107–118. [CrossRef]
69. ESGF Welcome to the ESGF Node @ IPSL. Available online: https://esgf-node.ipsl.upmc.fr/projects/esgf-ipsl/ (accessed on 27 November 2019).
70. EUROCORDEX CORDEX_variables_requirement_table. Available online: https://is-enes-data.github.io/CORDEX_variables_requirement_table.pdf. (accessed on 1 April 2018).
71. Kreienkamp, F.; Huebener, H.; Linke, C.; Spekat, A. Good practice for the usage of climate model simulation results—A discussion paper. *Environ. Syst. Res.* **2012**, *1*, 9. [CrossRef]
72. Dufresne, J.L.; Foujols, M.A.; Denvil, S.; Caubel, A.; Marti, O.; Aumont, O.; Balkanski, Y.; Bekki, S.; Bellenger, H.; Benshila, R.; et al. Climate change projections using the IPSL-CM5 Earth System Model: From CMIP3 to CMIP5. *Clim. Dyn.* **2013**, *40*, 2123–2165. [CrossRef]
73. Vrac, M.; Noël, T.; Vautard, R. Bias correction of precipitation through singularity stochastic removal: Because occurrences matter. *J. Geophys. Res.* **2016**, *121*, 5237–5258. [CrossRef]
74. Rasmus, B.; Andreas, H.; Barbara, H.; Tammas, I.; Daniela, J.; Elke, K.-T.; Sven, K.; Grigory, N.; Juliane, O.; Diana, R.; et al. *Guidance for EURO-CORDEX Climate Projections Data Use*. Available online: https://www.euro-cordex.net/imperia/md/content/csc/cordex/euro-cordex-guidelines-version1.0-2017.08.pdf (accessed on 1 April 2018).
75. Terray, L.; Boé, J. Quantifying 21st-century France climate change and related uncertainties. *Comptes Rendus Geosci.* **2013**, *345*, 136–149. [CrossRef]
76. ISO. *NF_EN_ISO_15927-2: Performance Hygrothermique des Bâtiments. Calcul et Présentation des Données Climatiques—Partie 2 Donnees Horaires Pour le Dimensionnement de la Charge de Refroidissement*; ISO: Geneva, Switzerland, 2009.
77. ASHRAE. *Ashrae Handbook Fundamentals*, SI ed.; ASHRAE: Peachtree Corners, GA, USA, 1997.
78. ISO. *ISO NF_EN_ISO_15927-1: Performance Hygrothermique des Bâtiments. Calcul et Présentation des Données Climatiques. Partie 1: Moyennes Mensuelles et Annuelles des Eléments Météorologiques Simples*; ISO: Geneva, Switzerland, 2004.
79. ASHRAE. *ASHRAE Fundamentals Handbook*; ASHRAE, Ed.; ASHRAE: Peachtree Corners, GA, USA, 2001.
80. Taesler, R.; Andersson, C. A method for solar radiation computations using routine meteorological observations. *Energy Build.* **1984**, *7*, 341–352. [CrossRef]
81. Young, A.T. Air mass and refraction. *Appl. Opt.* **1994**, *33*, 1108–1110. [CrossRef] [PubMed]
82. ISO. *ISO 15927-4: Performance Hygrothermique des Bâtiments. Calcul et Présentation des Données Climatiques. Partie 4: Données Horaires Pour L'évaluation du Besoin Energétique Annuel de Chauffage et de Refroidissement*; ISO: Geneva, Switzerland, 2006.
83. Robinson, P.J. On the definition of a heat wave. *J. Appl. Meteorol.* **2001**, *40*, 762–775. [CrossRef]
84. Nairn, J.; Fawcett, R. *Defining Heatwaves: Heatwave Defined as a Heat-Impact Event Servicing All Communiy and Business Sectors in Australia*; Centre for Australian Weather and Climate Research: Melbourne, Australia, 2013.

85. Nairn, J.R.; Fawcett, R.J.B. The excess heat factor: A metric for heatwave intensity and its use in classifying heatwave severity. *Int. J. Environ. Res. Public Health* **2014**, *12*, 227–253. [CrossRef] [PubMed]
86. Perkins, S.E.; Alexander, L.V. On the measurement of heat waves. *J. Clim.* **2013**, *26*, 4500–4517. [CrossRef]
87. Soubeyroux, J.-M.; Ouzeau, G.; Schneider, M.; Cabanes, O.; Kounkou-Arnaud, R. Les vagues de chaleur en France: Analyse de l'été 2015 et évolutions attendues en climat futur. *La Météorologie* **2016**, *8*, 45. [CrossRef]
88. Laaidi, K.; Ung, A.; Wagner, V.; Beaudeau, P.; Pascal, M. *The French Heat and Health Watch Warning System: Principles, fundamentals and assessment*; Institut de Veille Sanitaire: Saint-Maurice, Franch, 2013; Volume 20.
89. RTE. *Bilan Prévisionnel de L'équilibre Offre-Demande D'électricité en FRANCE*; RTE: Donnybrook, Ireland, 2017.
90. Cox, R.A.; Drews, M.; Rode, C.; Nielsen, S.B. Simple future weather files for estimating heating and cooling demand. *Build. Environ.* **2015**, *83*, 104–114. [CrossRef]
91. Arima, Y.; Ooka, R.; Kikumoto, H.; Yamanaka, T. Effect of climate change on building cooling loads in Tokyo in the summers of the 2030s using dynamically downscaled GCM data. *Energy Build.* **2016**, *114*, 123–129. [CrossRef]
92. Bravo Dias, J.; Carrilho da Graça, G.; Soares, P.M.M. Comparison of methodologies for generation of future weather data for building thermal energy simulation. *Energy Build.* **2020**, *206*, 109556. [CrossRef]
93. Van Hooff, T.; Blocken, B.; Hensen, J.L.M.; Timmermans, H.J.P. Reprint of: On the predicted effectiveness of climate adaptation measures for residential buildings. *Build. Environ.* **2015**, *83*, 142–158. [CrossRef]
94. Royé, D. The effects of hot nights on mortality in Barcelona, Spain. *Int. J. Biometeorol.* **2017**, *61*, 2127–2140. [CrossRef] [PubMed]
95. Guo, S.; Yan, D.; Hong, T.; Xiao, C.; Cui, Y. A novel approach for selecting typical hot-year (THY) weather data. *Appl. Energy* **2019**, *242*, 1634–1648. [CrossRef]
96. Coley, D.; Kershaw, T.; Eames, M. A comparison of structural and behavioural adaptations to future proofing buildings against higher temperatures. *Build. Environ.* **2012**, *55*, 159–166. [CrossRef]
97. Masson, V.; Marchadier, C.; Adolphe, L.; Aguejdad, R.; Avner, P.; Bonhomme, M.; Bretagne, G.; Briottet, X.; Bueno, B.; de Munck, C.; et al. Adapting cities to climate change: A systemic modelling approach. *Urban. Clim.* **2014**, *10*, 407–429. [CrossRef]
98. Machard, A.; Inard, C.; Alessandrini, J.-M.; Pelé, C.; Ribéron, J. Should we design buildings for future typical summers or future heatwaves? In Proceedings of the Windsor Conference, Windsor Great Park, UK, 16–19 April 2020.
99. Lapisa, R.; Bozonnet, E.; Salagnac, P.; Abadie, M.O. Optimized design of low-rise commercial buildings under various climates—Energy performance and passive cooling strategies. *Build. Environ.* **2018**, *132*, 83–95. [CrossRef]
100. Moazami, A.; Carlucci, S.; Nik, V.M.; Geving, S. Towards climate robust buildings: An innovative method for designing buildings with robust energy performance under climate change. *Energy Build.* **2019**, *202*, 109378. [CrossRef]
101. Campisi, D.; Gitto, S.; Morea, D. An evaluation of energy and economic efficiency in residential buildings sector: A multi-criteria analisys on an Italian case study. *Int. J. Energy Econ. Policy* **2018**, *8*, 185–196.
102. Ren, Z.; Chen, Z.; Wang, X. Climate change adaptation pathways for Australian residential buildings. *Build. Environ.* **2011**, *46*, 2398–2412. [CrossRef]
103. Perera, A.T.D.; Nik, V.M.; Chen, D.; Scartezzini, J.L.; Hong, T. Quantifying the impacts of climate change and extreme climate events on energy systems. *Nat. Energy* **2020**, *5*, 150–159. [CrossRef]